Zhang *et al. Cell Communication and Signaling* (2025) 23:245
https://doi.org/10.1186/s12964-025-02258-0

Cell Communication and Signaling

RESEARCH Open Access

ArcB initiates quorum sensing to regulate T3SS in *Vibrio alginolyticus* by recognizing bacterial and host-derived autoinducer-2 as a kinase

Ce Zhang[1], Xingkun Jin[1], Yan Shi[1], Fei Yu[1], Ying Wu[1], Douglas R. Call[2] and Zhe Zhao[1*]

Abstract

Background The marine pathogen *Vibrio alginolyticus* employs its type III secretion system (T3SS), a syringe-like secretion apparatus, to kill eukaryotic cells. Although the cascade regulation of the T3SS encoding ExsACDE operon has been described in detail for the *V. alginolyticus* T3SS, little is known about the signals and signaling pathways that regulate the operon.

Methods To investigate the regulation of T3SS by *V. alginolyticus* quorum sensing (QS) components, we measured lactate dehydrogenase (LDH) release following infection of Fathead minnow cells. A bioinformatics approach was employed to identify potential sensor kinases interacting with LuxU-LuxO. Bacterial two-hybrid assays were conducted to further elucidate interactions between these components. Phosphorylation and site-directed mutagenesis analyses were performed to delineate the phosphorelay system. The response of ArcB to autoinducer-2 (AI-2) or an AI-2 mimic was assessed using a Vibrio luminescence assay, and their interactions were quantitatively analyzed via microscale thermophoresis (MST) assays.

Results We observed that none of the three previously annotated sensing kinases in the *V. alginolyticus* QS system could regulate T3SS. Instead, the hybrid sensing kinase ArcB forms a signaling cascade with LuxU and LuxO to modulate T3SS expression. Furthermore, we confirmed that ArcB acts as a kinase in this pathway. Additionally, we found that ArcB can sense the LuxS-dependent autoinducer AI-2. Interestingly, host-derived AI-2 mimics produced during infection were also recognized by ArcB. Both signaling molecules activate the T3SS regulatory pathway.

Conclusions Our findings establish the ArcB-LuxU-LuxO signaling pathway as essential for the regulation of T3SS in *V. alginolyticus*. We further demonstrated that ArcB initiates this cascade by acting as a sensor for bacterial autoinducer-2, a signaling molecule involved in inter-species communication. Moreover, we show that host cells produce an AI-2 mimic during infection, which is also sensed by ArcB and can activate T3SS gene expression.

Keywords Quorum sensing, Autoinducer-2, AI-2 mimic, Type III secretion system, ArcB, *Vibrio alginolyticus*

*Correspondence:
Zhe Zhao
zhezhao@hhu.edu.cn

[1]Jiangsu Province Engineering Research Center for Marine Bio-resources Sustainable Utilization, College of Oceanography, Hohai University, Nanjing, Jiangsu, China
[2]Paul G. Allen School for Global Health, Washington State University, Pullman, WA, USA

Introduction

Type III secretion systems (T3SSs) are syringe-like structures located in the cell envelope of many gram-negative bacterial pathogens [1]. Cues from the environment and host sources can regulate transcription of T3SS genes. After injectisome assembly, this specialized structure translocates bacterial virulence factors, termed effector proteins, into eukaryotic target cells where they manipulate cellular processes and promote cell death [2]. *Vibrio parahaemolyticus* carries one T3SS on each of its two chromosomes, named T3SS1 and T3SS2, respectively. During infection, T3SS1 causes cytotoxicity, while T3SS2 is mainly associated with enterotoxicity [3–6]. The T3SSs of *V. parahaemolyticus* are highly regulated and activated under inducing conditions [7, 8]. For example, T3SS1 genes are positively regulated by the master regulator ExsA, a member of the AraC/XylS family of transcription factors, and the expression and activity of ExsA are then controlled by the ExsACDE partner-switching cascade [9]. Furthermore, the expression of *V. parahaemolyticus* T3SS1 is induced by contact of the bacteria with host cells [7], but the mechanism by which this contact signals upregulation of T3SS1 expression is still unknown.

Bacteria typically use two-component systems (TCSs) to detect environmental signals and trigger subsequent internal regulatory pathways to regulate gene expression. Signal transduction occurs via a phosphorylation-dephosphorylation mechanism [10] whereby a sensor kinase (SK) becomes phosphorylated on a conserved histidine residue in response to an environmental signal and subsequently transfers the phosphoryl group to an aspartic acid residue of a response regulator (RR) protein to elicit a specific cellular response [11]. Quorum sensing (QS) in *Vibrio* is controlled by a TCS. The QS process relies on the production, release, accumulation, and detection of extracellular signal molecules called autoinducers (AIs) [12].

ArcB was previously identified as a sensor kinase that functions in bacterial redox stress response [13]. In *V. parahaemolyticus*, ArcB still plays a canonical role under anaerobic conditions, while under aerobic conditions it replaces the function of phosphotransferase protein LuxU in the QS pathway and participates in the regulation of T3SS1 expression [14]. This finding underscores how ArcB is active in multiple conditions.

The autoinducer-2 (AI-2) can foster interspecies and inter-phyla communication, and its synthase (LuxS) is highly conserved and widespread in diverse bacteria [15, 16], while two AI-2 receptors (LuxP and LsrB) have been identified in various bacterial species. Both of these receptors are periplasmic-binding proteins belonging to the high-affinity substrate-binding protein family [17, 18]. Two novel AI-2 receptors with either a dCACHE domain or GAPES1 domain were recently discovered in bacteria [19, 20]. In *Pseudomonas aeruginosa*, AI-2 signaling is involved in chemotaxis and biofilm formation, although the bacterium neither produces AI-2 nor has canonical receptors. Instead, a transmembrane signal transduction protein with the dCACHE domain recognizes AI-2 and regulates the function of the coupled cytoplasmic effector region, ultimately causing a cellular response [19]. In *Salmonella enterica* serovar Typhimurium, AI-2 is independent of its known receptor LsrB but functions in biofilm formation and motility through another receptor carrying a GAPES1 domain [20].

As these examples illustrate, bacteria may possess multiple receptors that respond differentially to the same signal to regulate bacterial behavior. Recent evidence shows, however, that AI-2 is not confined to bacterial cell-to-cell communication, but also enables communication between bacteria and their hosts. Ismail et al. discovered that the colon, lung, and cervical mammalian cell lines produce a molecule mimicking AI-2 in response to bacterial cell factors and tight-junction disruption. This AI-2 mimic can be sensed by two AI-2 receptors, LuxP and LsrB, suggesting that the mimic binds at the same site as AI-2 and probably shares structural characteristics with it [21]. Moreover, *Saccharomyces cerevisiae* can produce an AI-2 mimic, 4-hydroxy-5-methylfuran-3(2 H)-one (MHF), but it is completely different from the AI-2 mimic secreted by mammalian cells [22]. These findings indicate that the AI-2 signaling pathway is widespread and may be a core of cross-domain communication.

Vibrio alginolyticus, a gram-negative halophilic bacterium found in marine and estuarine environments, causes varying degrees of disease in a variety of marine organisms [23, 24]. *V. alginolyticus* has been recognized as an emerging human pathogen, causing sepsis, superficial wounds, soft tissue infections, and extraintestinal infections [24, 25]. Given the significant and sustained threats posed by *V. alginolyticus* to both the global aquaculture industry and public health, it is important to better understand the virulence mechanisms of *V. alginolyticus*. Previous studies demonstrated that its pathogenesis likely involves the T3SS-mediated induction of rapid apoptosis, cell rounding and osmotic lysis of infected eukaryotic cells [26]. In addition, the expression of T3SS gene in *V. alginolyticus* is regulated by the *exsACDE* operon as has been observed in *V. parahaemolyticus*. Indeed, co-culture but not physical contact with host cells is sufficient to upregulate transcription of *exsA*, consistent with an external sensing system regulating the *V. alginolyticus* T3SS [27]. A *V. parahaemolyticus*-like QS signaling system has been characterized in *V. alginolyticus* [28, 29], but its regulatory effect on T3SS is still unknown.

Herein we demonstrated that the hybrid sensor kinase ArcB in *V. alginolyticus* coordinates with the

QS downstream components LuxU and LuxO by functioning as sensor protein, not as a histidine phosphotransfer (Hpt) protein, to form a new pathway (ArcB-LuxU-LuxO) that regulates T3SS. Importantly, ArcB not only senses bacterial AI-2 molecules, but it also recognizes an AI-2 mimic secreted by host cells when co-cultured with bacteria. ArcB then to initiates a phosphotransfer cascade in the ArcB-LuxU-LuxO pathway. These findings establish ArcB as a novel AI-2 receptor and elucidate the molecular mechanism through which host-derived factors activate *V. alginolyticus* T3SS in a contact-independent manner. This work expands our understanding of host-pathogen communication and reveals the complex strategies by which bacteria and host signals regulate infectivity.

Materials and methods

Bacterial strains, plasmids, and culture conditions

The *V. alginolyticus* strain ZJO is an opaque variant derived from the ZJ51 [30]. The *V. parahaemolyticus* strain RIMD 2,210,633 is a wild-type O3:K6 pandemic strain. For routine cultivation, *V. alginolyticus* was inoculated into trypticase soy broth (TSB) at 1% sodium chloride w/v or on thiosulfate citrate bile salts sucrose agar (TCBS; Huankai, China) at 30 °C. *V. parahaemolyticus* was inoculated into heart infusion broth (HI; BD, USA) at 1% sodium chloride w/v or on TCBS at 37 °C. For aerobic growth conditions, bacterial cultures were incubated in 12-ml tubes with loosely fitted caps and shaken at 200 rpm (high oxygen). For anaerobic conditions, bacteria were grown in tightly sealed 12-ml tubes without shaking (low oxygen). *Escherichia coli* DH5α served as the general cloning host for plasmid maintenance and propagation, *E. coli* S17-1 functioned as the donor strain for conjugation-mediated gene transfer, and *E. coli* BL21(DE3) was employed as the expression host for recombinant protein production. All *E. coli* strains were grown at 37 °C in Luria-Bertani (LB; BD, USA). Conjugates were selected on TCBS agar supplemented with 5 μg ml^{-1} chloramphenicol. For sucrose-based selection, trypticase soy agar (TSA) and TSB containing 10% (w/v) sucrose were utilized.

The construction of gene knockouts was performed using the suicide vector pDM4, whereas complementation studies were conducted with two distinct expression vectors: pMMB207 and pBBR1MCS-1. For cold-shock-induced protein expression, the specialized pCold I vector, which contains a cold-shock promoter *cspA*, was utilized to facilitate efficient expression of target proteins under low-temperature conditions. *V. alginolyticus* cultures were supplemented with ampicillin (100 μg ml^{-1}) or chloramphenicol (5 μg ml^{-1}) as needed. *E. coli* cultures were supplemented with ampicillin (100 μg ml^{-1}), chloramphenicol (25 μg ml^{-1}), and kanamycin (50 μg ml^{-1}). Details of all bacterial strains and plasmids utilized in this study are presented in Supplementary Table S1.

Generation of deletion mutants, complementation strains and Recombinant plasmids

All deletion mutants were constructed using allelic exchange, following a previously established method [31]. Deletion cassettes for in-frame chromosomal deletions were created using the splice-overlap-extension (SOE) PCR technique. This method fuses two PCR fragments (400–600 bp each) corresponding to the genomic regions flanking the target gene(s). The resulting deletion cassettes were subsequently cloned and inserted into the suicide vector pDM4 using the ClonExpress II one-step cloning kit (Vazyme, China). Following sequence verification, the recombinant vector was first transformed into the donor strain *E. coli* S17-1 and then transferred into *Vibrio* species through biparental conjugation. Transconjugants were selected on chloramphenicol-containing media, with resistant colonies indicating successful chromosomal integration through homologous recombination. To facilitate plasmid excision, positive clones were subsequently plated on sucrose-supplemented agar, allowing for counterselection. Mutant strains were identified based on their dual phenotype: sucrose resistance and chloramphenicol sensitivity. For the construction of $arcB^{Hpt}$, an SOE PCR strategy was implemented to generate a precise deletion cassette encompassing the Hpt domain coding sequence while preserving the native start codon of *arcB*.

For complementation studies, the promoter region and full open reading frame (ORF) of each target gene were cloned and inserted into the pBBR1MCS-1 vector. For Western blot analysis, the ORF of each gene was expressed with a C-terminal Flag tag under the control of the Ptac promoter in the pMMB207 vector. Site-directed mutagenesis was conducted using the Mut Express II Fast Mutagenesis Kit V2 (Vazyme, China) to introduce point mutations into the pBBR1MCS-1 and pMMB207 vectors, following the manufacturer's instructions. The mutagenized plasmids were subsequently verified by DNA sequencing before being transformed into *E. coli* S17-1.

For in vitro phosphorylation assays, *arcB*, *luxU*, and *luxO* were expressed in the pCold vector with N-terminal tags. Notably, the *arcB* construct was truncated (residues 78–784) to exclude the two transmembrane domains. For ArcB binding assays, the 5'-terminal sequence of *arcB* was cloned and inserted into the pCold vector to express the N-terminal region (amino acids 1-160) of ArcB.

All mutants and complementation strains were verified by PCR and DNA sequencing. Routine PCR was performed using Green Taq Mix (Vazyme, China), while preparative PCR for plasmid construction was carried out with PrimeSTAR® GXL Premix Fast (Takara, Japan),

following the manufacturer's protocols. All primers used in this study are listed in Table S2.

Identification of sensor kinase candidates with conserved domains

The genome and proteome data of *V. alginolyticus* (GCF_001679745.1) were downloaded from the NCBI database. Two sensor kinase (SK)-specific domains, HisKA (PF00512) and HATPase_c (PF02518), were obtained from the Pfam database. HMMER version 3.3.2 was used to search the *V. alginolyticus* proteome using the PF00512 and PF02518 domain models as queries, with a significance threshold of $e < 0.001$ to identify candidate SK genes.

LDH release assay

Fathead minnow (FHM) epithelial cells were maintained in Dulbecco's modified Eagle's medium (DMEM; Gibco, USA) containing 10% fetal bovine serum (FBS) at 27 °C. To assess cytotoxicity, confluent monolayers of FHM cells in 96-well plates were rinsed three times with pre-warmed phosphate-buffered saline (PBS) and then exposed to bacterial infections at a multiplicity of infection (MOI) of 100 for 2 h. For longer experiments lasting 7 h, the MOI was reduced to 20 to facilitate clearer imaging of cytotoxic effects.

After infection, culture supernatants were collected following centrifugation at 3000 ×*g* for 5 min. The lactate dehydrogenase (LDH) activity in the supernatants was quantified using the LDH Cytotoxicity Detection kit^{PLUS} (Roche, Germany). Absorbance readings were taken at 490 nm using a Tecan Spark microplate reader. The background LDH release from uninfected FHM cells was subtracted from the values obtained for infected cultures to calculate the percentage cytotoxicity. To determine the maximum LDH release, cells were lysed with Triton X-100. Uninfected cells served as negative controls for the assay.

Measurement of growth

The cultures to be tested were inoculated into fresh TSB medium. The growth was monitored at an optical density of 600 nm every 2 h, starting from the adaptation phase until the stationary phase, to construct growth curves. All assays were carried out in triplicate, with the entire experiment being repeated at least three times.

Protein expression and purification

Recombinant pCold plasmids were transformed into *E. coli* BL21(DE3) or BL21 (DE3) Δ*luxS* strains. The transformed cells were grown in LB broth supplemented with 100 μg/ml ampicillin at 37 °C with shaking. When the culture reached an OD_{600} of 0.6, it was rapidly cooled to 20 °C and maintained for 30 min. Then 0.5 mM isopropyl-β-D-thiogalactoside (IPTG) was added and incubated at 20 °C for 24 h with shaking to induce protein expression. After induction, 5–10 ml cultures were harvested by centrifugation at 5,000 ×*g* for 20 min. The cell pellets were resuspended in BugBuster Master Mix (Millipore, USA) at a ratio of 5 ml per gram of wet cell mass and incubated for 20 min at ambient temperature with gentle shaking. The lysates were clarified by centrifugation at 12,000 ×*g* for 30 min at 4 °C.

The supernatant was mixed with 2 ml of Ni-NTA Agarose (Qiagen, USA) and incubated at 4 °C for 12 h with constant gentle agitation at 20 rpm. The protein-resin mixture was then loaded onto a column, and the recombinant protein was purified using Ni-NTA affinity chromatography. The eluted fractions were analyzed by SDS-PAGE to assess protein recovery and purity, and the fractions containing the target protein were pooled. The purified protein was concentrated and subjected to buffer exchange using Amicon ultrafiltration (Millipore, USA) with a molecular weight cutoff appropriate for the target protein. The final storage buffer consisted of 50 mM Tris-HCl (pH 7.6), 0.1 mM EDTA, 100 mM KCl, 10 mM $MgCl_2$, and 30% (v/v) glycerol.

SDS-PAGE and Western blot analysis

Protein extracts from various strains were prepared using the BugBuster Master Mix. Protein samples were mixed with loading buffer, denatured through heat treatment for 10 min, and then resolved by SDS-PAGE. The separated proteins were transferred onto polyvinylidene difluoride membranes (Millipore, USA). The membranes were blocked overnight at 4 °C with 5% (w/v) nonfat dry milk dissolved in 1× Tris-buffered saline containing 0.1% Tween-20 (TBST) to prevent nonspecific binding. The primary antibodies (Proteintech, USA) were diluted 1:2,000 in 5% nonfat milk. The secondary antibody, goat anti-mouse IgG (H1L) conjugated to horseradish peroxidase (Proteintech, USA), was used at a 1:5,000 dilution. After each antibody incubation step, the membranes were washed three times with 1× TBST for 10 min per wash. Protein bands were detected using SuperSignal™ West Pico PLUS Chemiluminescent Substrate (Thermo Fisher Scientific, USA) and imaged with a FluorChem® E system (Cell Biosciences, USA). To quantify ArcB phosphorylation levels, ImageJ was used to analyze blot images. The phosphorylation fraction of ArcB was calculated on the basis of the band intensities of both phosphorylated and unphosphorylated forms.

Phosphorylation assays

For in vivo phosphorylation analysis, a Phos-tag-based mobility shift assay was performed. TCBS agar plates are used to isolate individual colonies of bacteria carrying a specific plasmid. Single colonies were inoculated

into TSB and induced with 1 mM IPTG for 3 h when the OD_{600} reached 0.5. Bacterial cells were harvested by centrifugation at 4,000 ×*g* for 10 min at 4 °C, and total proteins were extracted using BugBuster Master Mix according to the manufacturer's protocol. Protein samples were subsequently resolved on 8% (w/v) SDS-PAGE gels containing 20 μM Phos-tag reagent (Wako, Japan) and 40 μM $MnCl_2$. Phosphorylation-induced mobility shifts were detected by western blotting.

In vitro phosphorylation was conducted at ambient temperature. For autophosphorylation assays, purified proteins were diluted to a final concentration of 1 μM in kinase reaction buffer (50 mM Tris-HCl, pH 7.6, 100 mM KCl, and 10 mM $MgCl_2$). The phosphorylation reaction was added with 10 mM ATP for 10 min, and a 15-μl aliquot was collected and mixed with SDS-PAGE loading buffer (NCM Biotech, China) to terminate the reaction [32]. Proteins were resolved on 20 μM Phos-tag 8% SDS-PAGE, followed by western blot analysis using specific antibodies. For phosphotransfer analysis, excess ATP in ArcB ~ P buffer was removed by desalting, and a two-fold molar excess of LuxU and LuxO was added to reaction for 90 s. Reaction products were analyzed using the same phosphorylation assays as above.

Bacterial two-hybrid assays

Using bacterial adenylate cyclase two-hybrid system, proteins of interest were fused to the T18 and T25 domains of the adenylate cyclase. pKT25-zip/pUT18C-zip and pKT25/pUT18C served as positive and negative controls, respectively. The plasmids encoding the fusion proteins were co-transformed into the reporter strain BTH101 [33]. Transformed cells were plated on LB plates containing 100 μg ml^{-1} ampicillin, 50 μg ml^{-1} kanamycin, 0.5 mM IPTG, and 40 μg ml^{-1}X-gal and incubated at 30 °C for 12 h, with positive and negative controls used as references for recording colony color.

For quantitative β-galactosidase activity assays, BTH101 cultures were incubated overnight at 30 °C in LB broth containing 100 μg ml^{-1} ampicillin, 50 μg ml^{-1} kanamycin, and 0.5 mM IPTG, diluted to an OD_{600} = 0.05 and further incubated to 0.5. Bacterial cells from 200 μl of culture were pelleted and resuspended in 1 ml of Z buffer (60 mM Na_2HPO_4, 40 mM NaH_2PO_4, 10 mM KCl, and 1 mM $MgSO_4$, pH 7.0). To lyse the cells, 25 μl of chloroform and 25 μl of 0.1% SDS were added, followed by vigorous mixing. The reaction was initiated by adding 200 μl of o-nitrophenyl-β-D-galactoside (ONPG, 4 mg ml^{-1}). Until sufficient yellow color had developed, then 0.5 ml of 1 M Na_2CO_3 was added to each sample to stop the reaction. The samples were spun at 16,000 ×*g* for 5 min to remove debris and chloroform, and absorbance readings were measured at 420 nm to quantify β-galactosidase activity.

Quantitative real-time PCR

V. alginolyticus strains were grown aerobically in TSB supplemented with ampicillin or chloramphenicol for 5 h. A 2 ml aliquot of the culture was centrifuged at 8,000 ×*g* for 2 min. The resulting cell pellets were washed twice with sterile PBS and subsequently resuspended in 10 ml of DMEM containing 1% FBS. Following a 3-hour aerobic incubation, total RNA was isolated using TRIzol reagent (Invitrogen, USA). RNase-free DNase I (Thermo Fisher Scientific, USA) was used to remove the residual genomic DNA. cDNA was synthesized from the isolated RNA using a cDNA Synthesis Kit (Bio-Rad, USA).

Quantitative real-time PCR was performed on a LightCycler 96 system (Roche, Germany) using SYBR Green qPCR Master Mix (Takara, Japan). The sequences of the primers used for qPCR are listed in Table S2. The average cycle threshold values were normalized to the reference gene *rpoA*, and relative changes in gene expression were calculated using the $2^{-\Delta\Delta CT}$ method [34].

AI-2 assay

The AI-2 bioassay was performed according to the previously described methods [35] except we engineered the reporter strain *Vibrio harveyi* BB170 to knockout *cqsS*, resulting in strain BB180 ($LuxN^-$, $LuxPQ^+$, $CqsS^-$). *V. harveyi* was cultivated in modified autoinducer bioassay (AB) medium [36]. Overnight cultures of reporter strain *V. harveyi* BB180 were diluted to 1:5,000 in fresh AB medium and then 180 μL of bacterial culture was mixed with 20 μL of sample and incubated at 30 °C for 4 h. After incubation, 100-μL aliquots were added to white, flatbottomed, 96-well plates (Thermo Labsystems, USA) for detection of AI-2 activity. Sterile medium was used as the negative control. AI-2 activity is summarized as fold change for induction relative to that of the negative control. Luminescence was measured with a Tecan Spark microplate reader in luminescence mode. All samples were assayed in triplicate.

FHM cells co-culture with bacteria

FHM cells were cultured in 24-well culture plates in co-culture medium (1X DMEM without FBS) and grown to confluence (24 h, 27 °C). Overnight *V. alginolyticus* culture was diluted 1:100 in co-culture medium and 1 ml was added to the FHM cell culture or to the upper chamber of a transwell located above the cell monolayers. Following 5 h of co-culture, co-culture medium from the co-culture or the upper chamber of the transwell was assayed, in triplicate, for AI-2 or AI-2 mimic activity using the *V. harveyi* BB180 reporter strain.

Binding of Recombinant ArcB to AI-2

To determine whether the ArcB can bind to endogenous AI-2, the N-terminal region of ArcB (named exArcB) was

expressed in *E. coli* BL21 WT and BL21 Δ*luxS* strains using the pCold-$arcB^{1-160}$. After purification, two exArcB proteins were respectively named exArcB (BL21) and exArcB (BL21Δ*luxS*) to distinguish the sources. Next, exArcB (BL21) and exArcB (BL21Δ*luxS*) proteins (10 mg ml^{-1}) were incubated for 10 min at 60 °C to release endogenous AI-2. After incubation, the exArcB proteins were removed by ultrafiltration (10-KDa cut-off; Millipore), and the filtered reaction products were tested for AI-2 activity using a *V. harveyi* BB180 bioassay. All samples were assayed in triplicate.

To assess potential binding between exArcB and the AI-2 or AI-2 mimic, 10 mg ml^{-1} exArcB (BL21Δ*luxS*) was incubated with the cell-free supernatant containing bacteria AI-2 at room temperature. After incubation for 1 h, the exArcB protein was removed by ultrafiltration, and the filtered reaction products were tested for AI-2 activity using a *V. harveyi* BB180 bioassay to investigate the binding activity of exArcB to the bacterial AI-2. In addition, the exArcB protein was incubated with the collected cell-free supernatant from the co-culture of Δ*luxS* and FHM cells at room temperature for 1 h. The exArcB protein that captured the host AI-2 mimic was purified by Ni^{2+}-NTA affinity chromatography after incubation, and then replaced with the buffer containing 50 mM NaH_2PO_4 (pH 8.0), 300 mM NaCl and 1 mM DTT by Sephadex-G25 gel chromatography. After concentration by ultrafiltration, ligands were released from the denatured proteins by heating and the denatured proteins were removed by centrifugation to determine the relative activity of AI-2.

High-performance liquid chromatography (HPLC) assay

HPLC detection was performed on aqueous solutions containing AI-2 mimic and DPD/AI-2 standards by using an UltiMate 3000 UHPLC equipped with a C18 analytical column (100 mm ×2.1 mm) with 1.7 μm particle size (Thermo Fisher Scientific, USA). The mobile phase consisted of acetonitrile and water (80:20). The flow rate was 1 ml/min and the UV detection was set to 280 nm. The injection volume was 25 μL. The running time for each sample was 12 min.

Microscale thermophoresis (MST) assay

MST assays were performed to qualitatively examine the binding affinity between AI-2/AI-2 mimic and exArcB. Briefly, 10 μM exArcB was labeled with a fluorescent dye using the Protein Labeling Kit RED-NHS 2nd Generation (NanoTemper, Germany) and eluted in PBS buffer. Next, the labeled exArcB (20 nM) was respectively mixed with prepared gradient-diluted bacterial AI-2 or host-derived AI-2 mimic (2 μM to 0.000122 μM). After a short incubation at room temperature, the samples were centrifuged for 5 min at 16,000 ×g to remove large aggregates and then each was loaded into a premium capillary (NanoTemper, Germany). All measurements were performed using a Monolith Instrument NT.115 (NanoTemper, Germany) at a constant LED excitation power of 20% and an MST power of 40%. To estimate binding affinity, the dissociation constant K_d for each ligand was calculated using the NanoTemper Analysis software based on the changes in the normalized fluorescence (ΔFnorm [‰]) versus the ligand concentration.

Statistical analysis

The data are presented as means ± standard deviations. Multiple Student's *t*-test was used for comparisons between two groups. ANOVA was used for comparisons among multiple groups. *P*-values <0.05 were considered statistically significant. Analyses were conducted using GraphPad Prism Software (version 8.3.0).

Results

ArcB works together with LuxU and LuxO as a kinase to regulate *V. alginolyticus* cytotoxicity

To determine the potential involvement of *V. alginolyticus* quorum sensing in T3SS regulation, five single gene-deletion mutants that respectively disrupted five QS components [three sensor kinases (SKs): LuxQ, LuxN and CqsS, one Hpt protein: LuxU, one response regulator (RR): LuxO] were constructed and subjected to cytotoxicity assays by measuring LDH release after 2 h infection of Fathead minnow (FHM) cells. Unexpectedly, disruption of *luxQ*, *luxN* and *cqsS* did not affect *V. alginolyticus* cytotoxicity, while the deletion of either *luxU* or *luxO* caused a significant reduction in LDH release from infected host cells (Fig. 1A). *In trans* expression using plasmid-borne *luxU* or *luxO* in their corresponding mutant Δ*luxU* and Δ*luxO* successfully restored the LDH release level (Fig. 1A). These data indicated that three SKs in the *Vibrio* QS circuit were not involved in regulation of *V. alginolyticus* cytotoxicity, but their downstream proteins, LuxU and LuxO, were involved.

Considering that SKs play an essential role in the QS circuit, it is likely that other SKs in *V. alginolyticus* work with LuxU and LuxO to regulate cytotoxicity. To this end, 41 additional putative SKs were identified by genome-wide protein domain scanning (Fig. S1A), and their corresponding single-gene deletion mutants were generated. Cytotoxicity assays showed that, compared with the WT, only the BAU10_01410 (*arcB*) deletion mutant caused obviously decreased LDH release (Fig. S1B), and complementation of *arcB* restored the cytotoxic phenotype (Fig. 1B). Collectively, these findings confirm that ArcB, LuxU and LuxO are involved in the regulation of *V. alginolyticus* cytotoxicity.

To investigate whether ArcB operates within the same signaling pathway as LuxU and LuxO

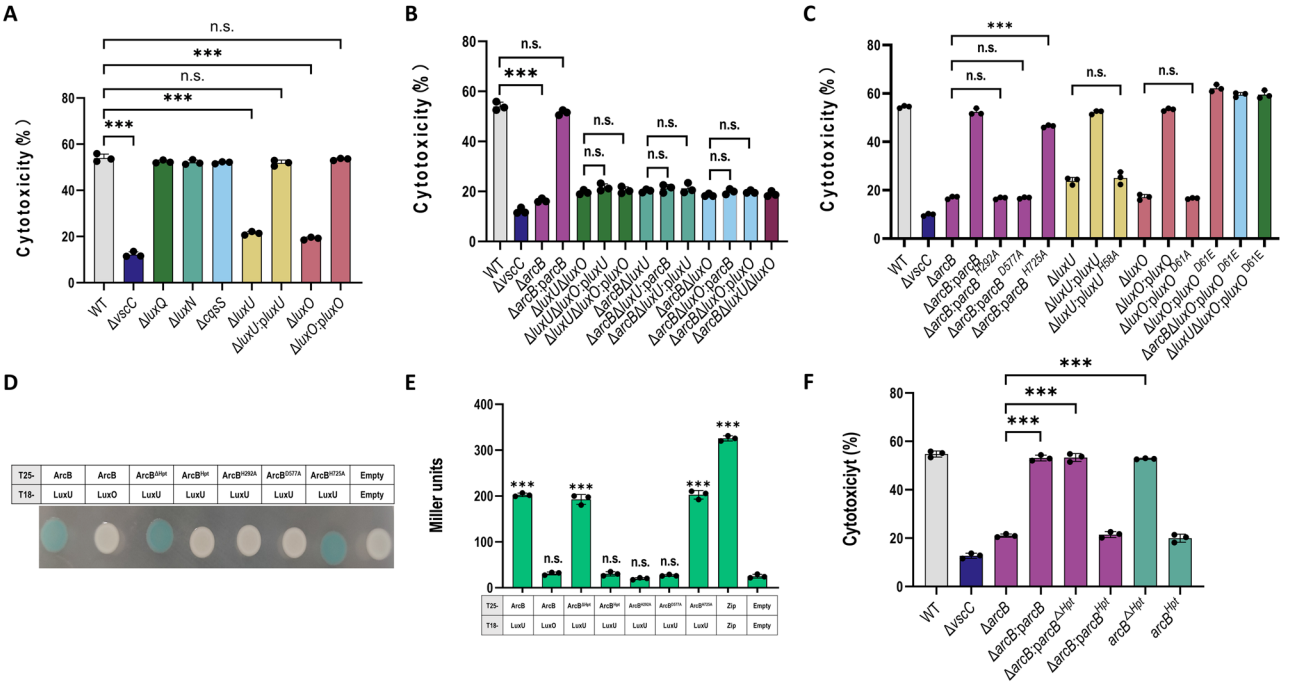

Fig. 1 ArcB works together with LuxU and LuxO as a kinase to regulate *V. alginolyticus* cytotoxicity. **(A-C**, **F)** LDH release assays (% cytotoxicity) of FHM cells infected with *V. alginolyticus* strains for 2 h, including the wild-type (WT) strain, indicated mutant strains, and complementation strains. The *vscC* gene encodes an outer membrane structural protein. Δ*vscC* is used as a T3SS-deficient control. Data are presented as means ± SD from three independent experiments. Statistical significance was determined using unpaired two-tailed *t*-test. ***$P < 0.0005$; n.s. not significant. **(D)** Bacterial two hybrid assay. Plasmid vectors carrying the indicated T18 and T25 constructs were transformed into BTH101. Individual colonies were grown in LB at 30°C for 12 h, then patched on LB medium supplemented with ampicillin (Amp), kanamycin (Kan), X-Gal, and 0.5 mM IPTG. Plates were incubated at room temperature for at least 12 h. T25 & T18 empty vectors as negative controls. Data shown represent one of three independent experiments with similar results. **(E)**β-galactosidase activity assay. A 1% inoculum of overnight bacterial culture was added to fresh medium, and β-galactosidase activity was measured at an OD_{600} to 0.6. The Miller unit was defined as the unit of β-galactosidase activity in the culture. T25-zip & T18-zip served as positive controls, and T25 & T18 empty vectors as negative controls. Data are presented as means ± SD from three independent experiments. Statistical significance was determined using one-way ANOVA. ***$P < 0.0005$; n.s. not significant

to regulate *V. alginolyticus* cytotoxicity, we constructed three double-deletion strains (Δ*arcB*Δ*luxU*, Δ*arcB*Δ*luxO*, and Δ*luxU*Δ*luxO*) and a triple-deletion strain(Δ*arcB*Δ*luxU*Δ*luxO*), and evaluated their cytotoxic effects. As expected, the LDH release caused by all the double- and triple- deletion mutants was reduced to levels comparable to those of single-deletion mutants (Fig. 1B). Furthermore, attempts to restore cytotoxicity by complementing any single gene in these double-deletion strains were unsuccessful (Fig. 1B). These findings indicate that ArcB probably coordinates with LuxO and LuxO within the same signaling pathway to modulate the cytotoxicity of *V. alginolyticus*.

The ArcB of *V. alginolyticus* is a hybrid sensor kinase whose intracellular region harbors three conserved domains: a histidine kinase A (HisKA) domain containing the conserved His^{292} residue, a central receiver (REC) domain with the conserved Asp^{577} residue, and a C-terminal Hpt domain bearing the conserved His^{725} residue (Fig. S2A). To elaborate the precise role of ArcB, we generated point mutations in plasmid-borne *arcB* and evaluated their cytotoxicity. LDH release assays revealed that complementation of $ArcB^{H725A}$ in the Hpt domain, but not $ArcB^{H292A}$ or $ArcB^{D577A}$ in the HisKA domain or REC domain, respectively, restored cytotoxicity of Δ*arcB* strain (Fig. 1C). Similarly, we constructed two point-mutations in histidine 58 within the Hpt domain of LuxU and aspartate 61 within the REC domain of LuxO and found they are both essential for regulatory function (Fig. 1C). Moreover, we generated a complemented mutant strain (Δ*luxO*:p*luxO*^{D61E}) designed to mimic the phosphorylated state, thereby locking LuxO in a constitutively active configuration [37]. This was done by mutating aspartate 61 to glutamate in LuxO. Δ*luxO*:p*luxO*^{D61E} retained cytotoxicity equivalent to that of the WT strain, and this effect was observed regardless of the presence or absence of ArcB or LuxU (Fig. 1C). From the above results, we surmise that the *V. alginolyticus* ArcB employs histidine kinase activity (HisKA domain and REC domain) to regulate cytotoxicity, while LuxU and LuxO are also essential for cytotoxicity. Furthermore, a phosphorelay may occur among them. To investigate whether ArcB physically interacts through a LuxU or LuxO phosphorelay, bacterial two-hybrid assays were conducted.

Results demonstrate that there is a direct interaction between ArcB and LuxU based on colony color (blue-green, Fig. 1D) and quantitative assessment (Fig. 1E). In contrast, no interaction was detected between ArcB and LuxO (Fig. 1D and E). Mutations on histidine 292 and aspartate 577 ($ArcB^{H292A}$ and $ArcB^{D577A}$), but not histidine 725 ($ArcB^{H725A}$) of ArcB, resulted in the disappearance of the interaction phenotype (Fig. 1D and E), which is consistent with the phosphorelay between ArcB and LuxU requiring physical interaction. The N-terminus of ArcB containing both HisKA and REC domains named $arcB^{\Delta Hpt}$, and the C-terminus containing only the Hpt domain, named $arcB^{Hpt}$, were complemented into the Δ*arcB* using the pMMB207, followed by cytotoxicity assays. Complementation of $arcB^{\Delta Hpt}$, but not $arcB^{Hpt}$, recovered cytotoxicity of the Δ*arcB* strain (Fig. 1F), and demonstrated a direct interaction with LuxU (Fig. 1D and E). We constructed a mutant $arcB^{\Delta Hpt}$ by deleting Hpt domain sequence so that the resulting ArcB included only the HisKA and REC domains. This strain exhibited similar cytotoxicity to that of the WT (Fig. 1F). Taken together, we concluded that the *V. alginolyticus* ArcB exerts kinase activity and initiates a new signaling pathway with LuxU and LuxO to regulate cytotoxicity.

Phosphotransfer cascade occurs in the ArcB-LuxU-LuxO pathway

We determined that there are four putative phosphorylation sites in ArcB, LuxU and LuxO (His^{292}, Asp^{577}, His^{58}, and Asp^{61}, respectively) that are essential for regulating *V. alginolyticus* cytotoxicity. To independently verify their phosphorylation status in vivo, the WT or mutant gene for each was overexpressed using the pMMB207 vector. For ArcB phosphorylation, C-terminal FLAG-tagged WT ArcB or three-point mutated ArcB were overexpressed in the Δ*arcB* strain. Phos-tag mobility shift assays revealed two bands when WT ArcB or $ArcB^{H725A}$ was expressed, but only the lower band was visible when $ArcB^{H292A}$ and $ArcB^{D577A}$ were expressed (Fig. 2A). In contrast, conventional polyacrylamide gels showed only the lower band for all strains, serving as a negative control. These results demonstrate that ArcB phosphorylation relies on a conserved histidine in the HisKA domain and a conserved aspartate in the REC domain. With respect to LuxU and LuxO phosphorylation, LuxU phosphorylation was absent in the Δ*arcB* strain, and LuxO phosphorylation was undetectable in the Δ*luxU* strain (Fig. 2B and C). Furthermore, histidine 58 in the LuxU Hpt domain and aspartic acid 61 in the LuxO REC domain were essential

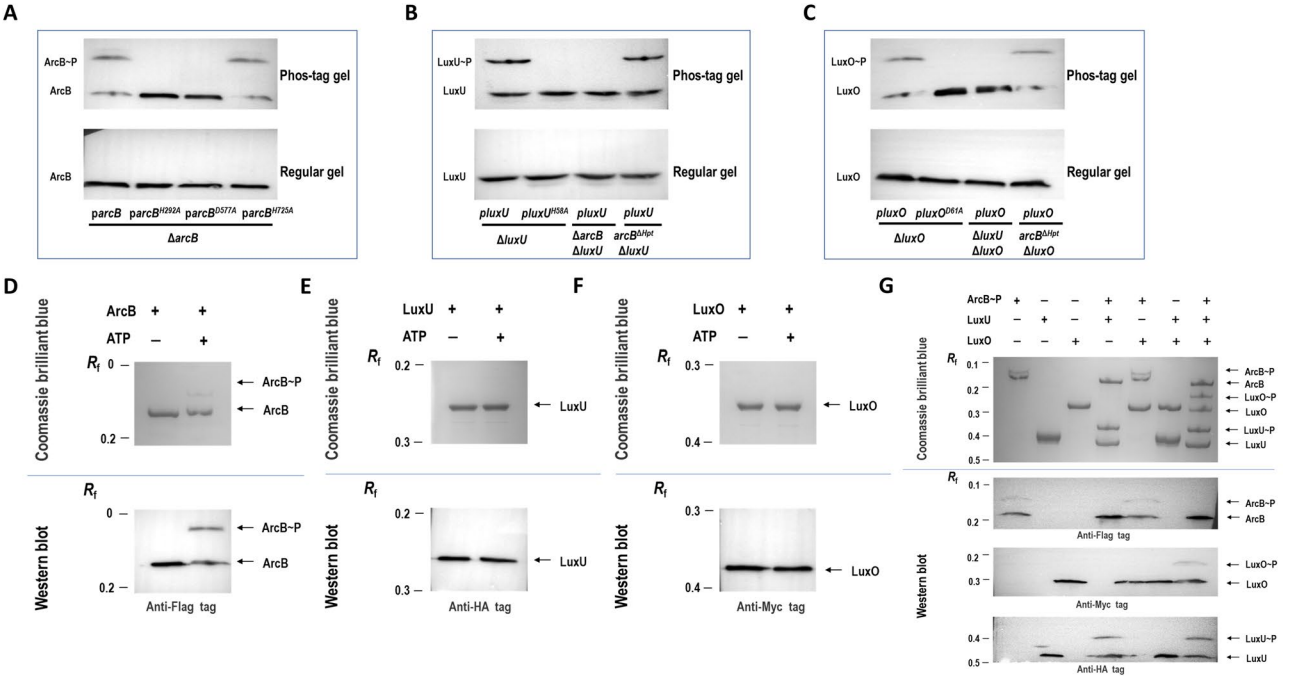

Fig. 2 Phosphotransfer cascade occurs in the ArcB-LuxU-LuxO pathway. **(A-C)** In vivo phosphorylation assays. The pMMB207 plasmid was used to construct all overexpressed strains as indicated in western blot analysis, and each gene was added a Flag tag to the C-terminus. Western blot analysis of *V. alginolyticus* cell lysates was performed using 8% SDS-PAGE with 20 μM Phos-tag to detect phosphorylation (upper panels; ArcB ~ P, LuxU ~ P and LuxO ~ P) and conventional 8% SDS-PAGE for total protein detection (lower panels). **(D-F)** In vitro phosphorylation assays. Phos-tag SDS-PAGE analysis of ArcB, LuxU and LuxO autophosphorylation reactions. Protein samples after autophosphorylation reactions were loaded onto 8% SDS-PAGE with 20 μM Phos-tag (upper panel), or subjected to immunoblotting with anti-Flag (ArcB), the anti-HA (LuxU) and anti-Myc (LuxO) antibodies (lower panels). **(G)** Phos-tag SDS-PAGE analysis of the ArcB/LuxU/LuxO phosphotransfer reactions. Phosphorylated ArcB (ArcB-P) was added to purified LuxU and LuxO to initiate phosphorylation transfer reactions. The reaction samples were loaded onto 8% SDS-PAGE with 20 μM Phos-tag (upper panel), or subjected to immunoblotting with specific antibodies for each protein (lower panels). Data shown are representative of three independent experiments with similar results

for phosphorylation because neither mutated protein was phosphorylated even in the presence of ArcB (Fig. 2B and C). We conclude that phosphorylation occurs at conserved sites for ArcB, LuxU, and LuxO, and further that ArcB is essential for the phosphorylation of LuxU and LuxO. Additionally, when LuxU and LuxO were overexpressed in the arcB$^{\Delta Hpt}$ strain, they were still phosphorylated (Fig. 2B and C), further supporting the hypothesis that ArcB functions as a kinase that regulates synthesis of LuxU and LuxO.

To further elucidate the phosphorelay mechanism involving ArcB, LuxU, and LuxO, we expressed and purified recombinant ArcB, LuxU, and LuxO proteins with distinct N-terminal tags and performed in vitro autophosphorylation and phosphotransfer assays. Phos-tag gel results showed that upon addition of ATP, an additional band appeared above the ArcB band (Fig. 2D, upper panel). Western blot analysis confirmed that this upward-shifted band was recognized by the ArcB tag antibody (anti-Flag antibody) (Fig. 2D, lower panel), demonstrating that ArcB undergoes autophosphorylation in the presence of ATP. In contrast, neither LuxU nor LuxO exhibited autophosphorylation activity with addition of ATP (Fig. 2E and F). We subsequently conducted a phosphate transfer analysis from phosphorylated ArcB to LuxU and LuxO (Fig. 2G). When phosphorylated ArcB was present, shifted Phos-tag bands of both LuxU and LuxO were observed (2G, upper panel), with specificity confirmed by western blotting using antibodies targeting their respective N-terminal tags (2G, lower panel). Overall, we conclude that the *V. alginolyticus* ArcB undergoes autophosphorylation, then transfers the phosphate group successively to the Hpt protein LuxU and the RR protein LuxO.

The ArcB-LuxU-LuxO pathway exerts cytotoxicity under aerobic conditions by regulating T3SS expression

V. alginolyticus cytotoxicity against host cells is T3SS-dependent and is characterized by rapid apoptosis, cell rounding and osmotic lysis (LDH release) [26]. Activation of caspase-3 is a hallmark of apoptosis and consequently we assayed caspase-3 activity in infected cells. The caspase-3 activity was significantly lower in cells infected with strains Δ*arcB*, Δ*luxU* or Δ*luxO* than in those infected with the WT strain (Fig. S2B), indicating the ArcB-LuxU-LuxO pathway probably controls global transcription of *V. alginolyticus* T3SS. For this purpose, several *V. alginolyticus* T3SS genes were included in the assay (translocons *vopB* and *vopD*, the regulators *exsA* and *exsD*, the effectors *val1686* and *val1680*, and structural proteins *vscY* and *vseE*). Compared with those of the wild-type strain and complementation strains (Δ*arcB*:BBR-*arcB*, Δ*luxU*: BBR-*luxU* and Δ*luxO*: BBR-*luxO*), the transcription levels of these genes were significantly downregulated in the single-deletion strains (Δ*arcB*, Δ*luxU* and Δ*luxO*) (Fig. 3A, B and S3). Complementation of mutations to amino acid residues involved in phosphate group transfer for ArcB, LuxU and LuxO (Δ*arcB*:BBR-*arcB*^{H292A}, Δ*arcB*:BBR-*arcB*^{D577A}, Δ*luxU*:BBR-*luxU*^{H58A} and Δ*luxO*:BBR-*luxO*^{D61A}) did not restore the transcription levels of those genes, whereas the mutation of histidine 725 (H725A) in the Hpt domain of *arcB* had a complementary effect (Figs. 3A, B and S3). When LuxO was maintained at a constitutively active status by complementing the *luxO*^{D61E}, the T3SS gene transcription levels increased, which was independent of the presence of ArcB or LuxU (Fig. 3A, B and S3). Collectively, these results suggest that the novel pathway ArcB-LuxU-LuxO controls cytotoxicity of *V. alginolyticus* by regulating T3SS expression.

The ArcB/ArcA two-component system is known to mediate adaptation to anaerobic growth conditions in *E. coli* [13]. It is interesting that ArcB orchestrated the QS components LuxU and LuxO to regulate *V. alginolyticus* T3SS under aerobic conditions, yet its cognate response regulator ArcA did not participate in this process, as evidenced by the cytotoxicity and gene transcription of the T3SS in *arcA* deletion mutant (Fig. 3A-C). To verify whether ArcB still fulfills its canonical role in anaerobic regulation in *V. alginolyticus*, we examined the phosphorylation status of the ArcB/ArcA in response to aerobic and anaerobic treatments. Phos-tag assays showed that the phosphorylated bands of ArcB were observed under both anaerobic and aerobic culture conditions, however, the phosphorylated ArcA appeared only under anaerobic conditions and in the presence of ArcB (Fig. 3D). These results indicate that ArcB can still function as a sensor histidine kinase to regulate anaerobic adaptation of *V. alginolyticus* by transferring the phosphate group to ArcA, but under aerobic conditions, ArcB switches to phosphorylate the downstream Hpt protein LuxU and response regulator LuxO to control T3SS expression.

ArcB initiates the new pathway by sensing bacterial AI-2 to regulate T3SS expression

Given that ArcB acts as sensor kinase with LuxU and LuxO to form a previously undescribed regulatory pathway, determining whether this SK can recognize the well-known QS signaling molecules in *Vibrio* species would be useful. Three deletion mutants of the QS molecule synthesis genes *luxM*, *luxS*, and *cqsA* (responsible for the biosynthesis of AI-1, AI-2, and CAI-1, respectively) were constructed, and LDH release assays after in vitro infection revealed that only the deletion of *luxS* caused significantly reduced cytotoxicity (Fig. 4A). The double mutant Δ*luxS*Δ*arcB* exhibited the same cytotoxic phenotype as the single mutant Δ*arcB*, suggesting that AI-2 may be ArcB-dependent when regulating T3SS. Importantly, our

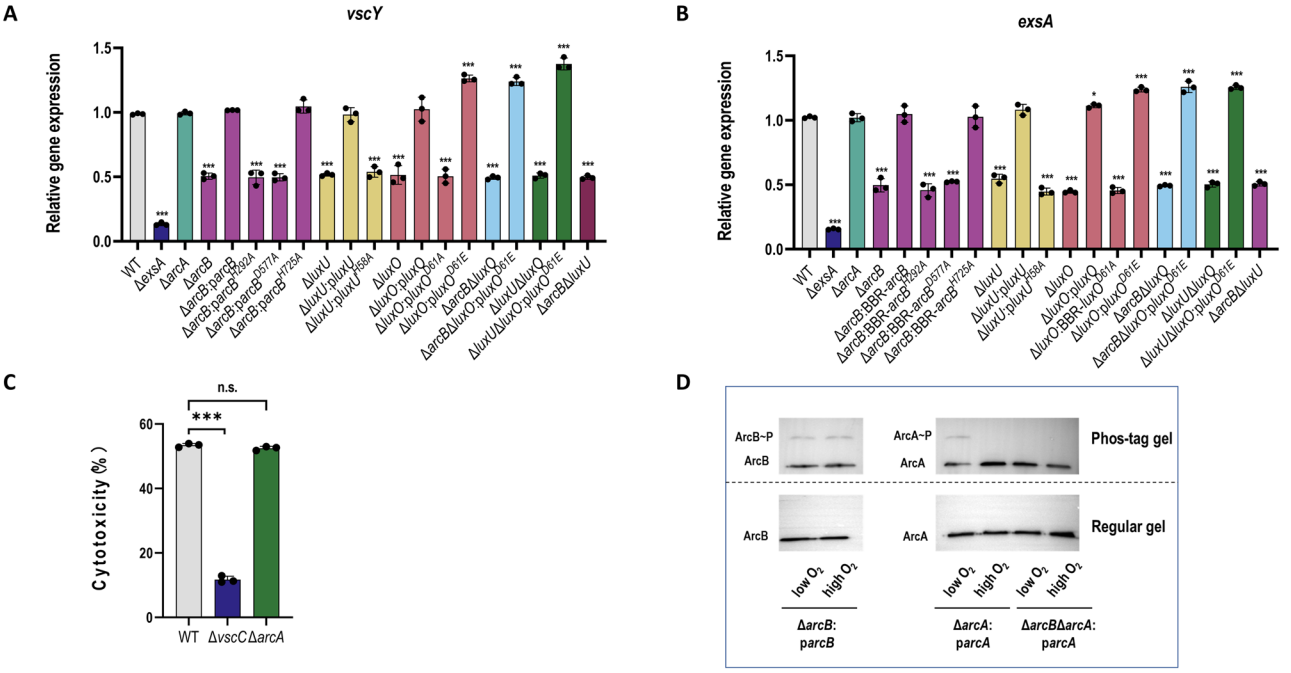

Fig. 3 The ArcB-LuxU-LuxO pathway exerts cytotoxicity under aerobic conditions by regulating T3SS expression. **(A, B)** Transcriptional levels of the T3SS genes *vscY* (structural protein gene) and *exsA* (regulator gene) in the indicated strains using qPCR. The data were normalized to *rpoA* expression. The pBBR1MCS-1 plasmid was used to construct for all the complemented strains. Data are presented as means ± SD from three independent experiments. Statistical significance was determined using one-way ANOVA. **P* < 0.05;****P* < 0.0005; n.s. not significant. **(C)** LDH release assays (% cytotoxicity) of FHM cells infected with the WT, Δ*vscC* and Δ*arcA* strains for 2 h. Data are presented as means ± SD from three independent experiments. Statistical significance was determined using one-way ANOVA. ****P* < 0.0005; n.s. not significant. **(D)** In vivo detection of ArcB (left panels) and ArcA (right panels) phosphorylation levels under high and low oxygen conditions. Western blot analysis of *V. alginolyticus* cell lysates was performed using Phos-tag™ to detection phosphorylation (upper panels; ArcB ~ P, ArcA ~ P) and conventional SDS-PAGE for total protein detection (lower panels). Data shown are representative of three independent experiments with similar results

in vivo phosphorylation assays at various growth stages found that ArcB phosphorylation is cell density-dependent, but in the absence of AI-2, ArcB was not phosphorylated during the time examined (Fig. 4B). Additionally, we conducted cytotoxicity assays by using cell-free supernatants (CFSs) from the cultured low-cell density phase WT (WT*cfs*) and Δ*luxS* (*luxScfs*) by replacing the culture medium upon infection. Compared to *luxScfs*, WT*cfs* enhanced cytotoxicity of WT and Δ*luxS*, but this effect was lost when *arcB* was deleted (Fig. 4C). Similarly, the addition of 1 μM DPD/AI-2 significantly increased the cytotoxicity of the Δ*luxS* strain but had no effect on the strain in which *arcB* was deleted (Fig. 4D). The above results revealed that the QS molecule AI-2 is required for ArcB phosphorylation and is therefore involved in the regulation of T3SS.

To investigate whether ArcB can bind to AI-2, the N-terminal fragment of ArcB, including extracellular and transmembrane regions (exArcB), was expressed and purified from *E. coli* BL21 WT and Δ*luxS* strain, respectively. After heat denaturation, the supernatants containing the released ligands were subjected to the bioluminescence assay in *V. harveyi* reporter strain BB180, showing that the supernatant derived from the BL21 WT strain (AI-2$^+$) induced strong luminescence, while supernatant from the BL21 Δ*luxS* strain (AI-2$^-$) did not (Fig. 4E), indicating the presence of AI-2 binding in the purified exArcB from *E. coli* WT extract. Further, in vitro binding of exArcB with AI-2 was assessed using the exArcB from the *E. coli* Δ*luxS* strain and the CFS from cultured *V. alginolyticus* ZJO. The bioluminescence assay revealed AI-2 activity in the supernatant after exArcB incubation was lower than that in normal supernatant (Fig. 4F). As a negative control, LuxO was included with the in vitro binding assay, showing no effect on AI-2 activity (Fig. 4F). Taken together, these findings indicate that ArcB initiates its autophosphorylation by sensing the LuxS-dependent autoinducer AI-2 to regulate T3SS in *V. alginolyticus*.

The AI-2 mimic produced by host cells regulates T3SS through ArcB

Earlier works have shown that co-culture with host cells, but not physical contact, can activate the T3SS of *V. alginolyticus* [27], however, it is still unclear how host cells signal this upregulation. Our results show that the bacterial AI-2 is involved in regulation of T3SS cytotoxicity by activating the ArcB-mediated pathway. Notably, the deletion of *luxS* caused reduced cytotoxicity, but

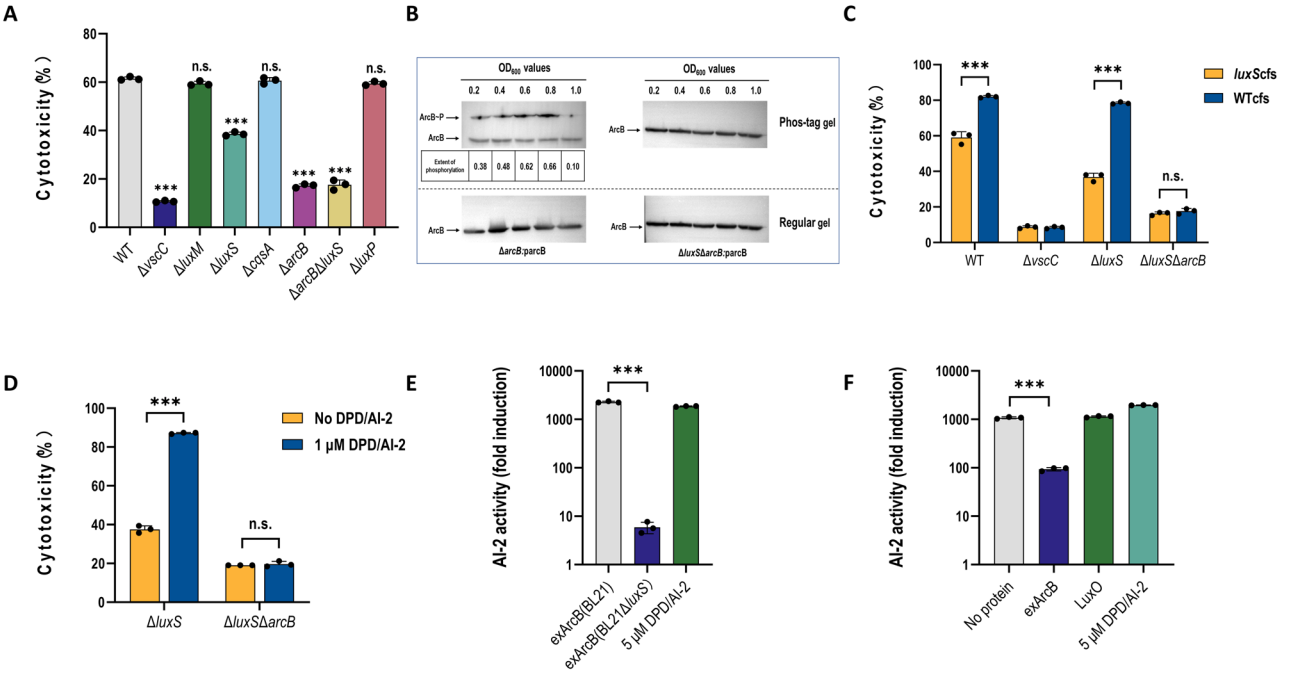

Fig. 4 ArcB initiates the new pathway by sensing bacterial AI-2 to regulate T3SS expression. **(A)** LDH release assays (% cytotoxicity) of FHM cells infected with the WT and mutant strains for 2 h. Data are presented as means ± SD from three independent experiments. Statistical significance was determined using one-way ANOVA. ***$P < 0.0005$; n.s. not significant. **(B)** In vivo phosphorylation of ArcB is cell density-dependent. Phosphorylation levels of ArcB were detected in strains Δ*arcB*:p*arcB* and Δ*luxS*Δ*arcB*:p*arcB* at various growth stages (OD_{600} of 0.20, 0.40, 0.60, 0.80, 1.00). Protein levels were normalized using RNA-Pol β. Data shown are representative of three independent experiments with similar results. **(C)** LDH release assays (% cytotoxicity) of FHM cells infected with WT and indicated mutant strains under two different CFSs for 2 h. Upon infection, the cell culture media were immediately replaced by the CFS collected from WT (WTcfs; blue bars) or Δ*luxS* (*lux*Scfs; yellow bars). Data are presented as means ± SD from three independent experiments. Statistical significance was determined using two-tailed multiple *t*-test. ***$P < 0.0005$; n.s. not significant. **(D)** LDH release assays (% cytotoxicity) of FHM cells infected with Δ*luxS* and Δ*luxS*Δ*arcB* strains for 2 h, with (blue bars) or without (yellow bars) the addition of 1 μM DPD/AI-2 at the beginning of infection. Data are presented as means ± SD from three independent experiments. Statistical significance was determined using two-tailed multiple *t*-test. ***$P < 0.0005$; n.s. not significant. **(E, F)** AI-2 activity assays using the AI-2 reporter *V. harveyi* strain BB180. In panel (E), exArcB (BL21) indicates that exArcB was expressed and purified in *E. coli* BL21 WT ($AI\text{-}2^+$) while exArcB (BL21Δ*luxS*) was from BL21Δ*luxS* ($AI\text{-}2^-$) strain. Then two purified proteins were heated for releasing ligands to supernatant. AI-2 activity in the supernatant was detected by incubating with the reporter strain BB180 and measuring bioluminescence production. 5 μM DPD/AI-2 solution was used as a positive control. In panel (F), purified exArcB or LuxO from BL21Δ*luxS* ($AI\text{-}2^-$) was incubated in CFS of *V. alginolyticus*, and then they were removed by ultrafiltration. AI-2 activity in the supernatant was detected by measuring bioluminescence production after incubation with the reporter strain BB180. Media without incubation with protein and 5 μM DPD/AI-2 solution were used as controls. AI-2 activity is reported as fold induction of bioluminescence over the background obtained in the buffer control alone. Data are presented as means ± SD from three independent experiments. Statistical significance was determined using one-way ANOVA. ***$P < 0.0005$

less than the deletion of *arcB* (Fig. 4A), indicating that ArcB may recognize other signaling molecules including potentially from host cells. To distinguish the effects of host cell signals, we performed time-course cytotoxicity assays at a reduced multiplicity of infection (MOI = 20). While the Δ*luxS* mutant initially showed reduced cytotoxicity compared to the WT, its virulence recovered to WT levels within 3 h post-infection (Fig. 5A). In contrast, the Δ*arcB*Δ*luxS* exhibited prolonged cytotoxicity suppression, with significantly delayed virulence recovery (Fig. 5A). Meanwhile, we examined the growth kinetics of various bacterial strains. The growth patterns of the Δ*luxS* and Δ*arcB*Δ*luxS* were comparable to that of the WT, except for a minor growth lag (~2 h) observed in the Δ*arcB*Δ*luxS* (Figure S4A). These results ruled out potential cytotoxicity differences attributable to growth variations among the mutants (Fig. S4A). These findings are consistent with the presence of unrecognized AcrB-dependent signaling molecules from the host cells that may serve a role similar to bacterial AI-2.

Further work using the bioluminescence assay showed that the CFS from the Δ*luxS* strain likely did not contain AI-2, whereas the CFS from co-culture of Δ*luxS* strain with host cells produced strong bioluminescence equivalent to what was observed for the WT or addition of 5 μM DPD/AI-2 (Fig. 5B). Cytotoxicity assays also revealed that the CFS from co-culture of Δ*luxS* strain with host cells enhanced the cytotoxic phenotype of the WT and Δ*luxS* strains, whereas the mono-culture medium from host cells alone had no effect (Fig. 5C). Phosphorylation detection of ArcB in the Δ*luxS*Δ*arcB*:p*arcB* strain also supported the above findings, as evidenced by the lack of ArcB

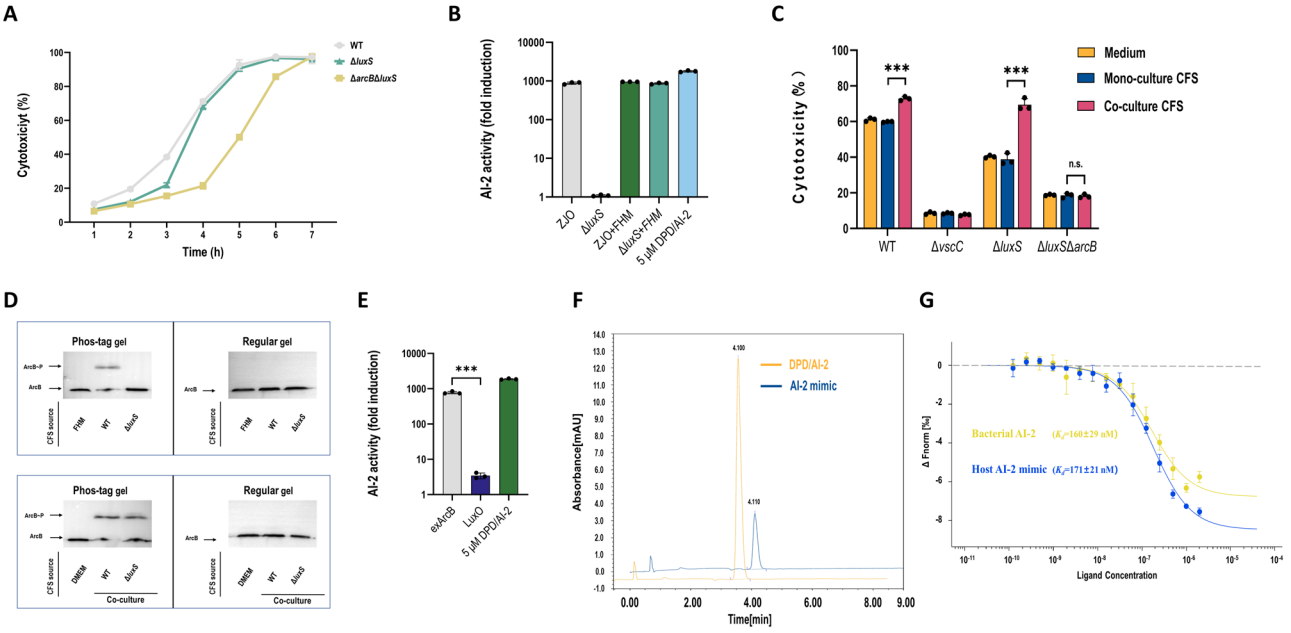

Fig. 5 The AI-2 mimic produced by host cells regulates T3SS through ArcB. **(A)** Time-course analysis of LDH release (% cytotoxicity) in FHM cells infected with different strains. At the indicated time points, LDH release in the culture supernatants was measured, and cytotoxicity was calculated as a percentage of total cellular lysis, including WT (circle), Δ*luxS* (triangle), and Δ*arcB*Δ*luxS* (square). **(B)** AI-2 activity assays for CFSs from co-cultures of FHM cells with *V. alginolyticus* WT and Δ*luxS* strains using the AI-2 reporter *V. harveyi* strain BB180. As control, *V. alginolyticus* WT and Δ*luxS* strains were also cultured in DMEM medium and their CFSs were included. A 5 μM DPD/AI-2 solution served as a positive control. **(C)** LDH release assays (% cytotoxicity) of FHM cells infected with the indicated strains under different conditioned culture media for 2 h. Upon infection, the cell culture media were immediately replaced by the CFS from FHM mono-culture (blue bars) or co-culture (pink bars) with *V. alginolyticus* Δ*luxS* strain. Replace the normal medium (yellow bars) as the control. Data are presented as means ± SD from three independent experiments. Statistical significance was determined using two-tailed multiple *t*-test. ***$P < 0.0005$; n.s. not significant. **(D)** In vivo phosphorylation assays of ArcB under different conditioned culture media. The Δ*luxS*Δ*arcB*:*parcB* strain was respectively grown for 1 h in CFS collected from host cells, *V. alginolyticus* WT and Δ*luxS* cultures (upper panel), or CFS from co-culture of FHM cells with *V. alginolyticus* WT and Δ*luxS* strain (lower panel). DMEM medium was included as negative controls. Phosphorylated band of ArcB was detected by Phos-tag SDS-PAGE. Data shown are representative of three independent experiments with similar results. **(E)** The capture of host AI-2 mimic by the exArcB. Recombinant exArcB obtained from *E. coli* BL21Δ*luxS* (AI-2$^-$) was incubated in the CFS from the co-culture of *V. alginolyticus* Δ*luxS* and FHM cells. The exArcB was then re-purified, and denatured by heating to release the bindings. Afte r centrifugation to remove denatured proteins, the supernatant was subjected to measure bioluminescence production using the reporter strain BB180. LuxO as control was included and performed as exArcB. A 5 μM DPD/AI-2 solution was included as a positive control. Data are presented as means ± SD from three independent experiments. Statistical significance was determined using one-way ANOVA. ***$P < 0.0005$. **(F)** Chromatogram depicting DPD/AI-2 and AI-2 functional analogue. The chromatograms show absorption at 280 nm. mAU, milli-absorbance units. **(G)** The exArcB specifically binds to bacterial AI-2 or host AI-2 mimic with high affinity. The exArcB was obtained from *E. coli* BL21Δ*luxS* (AI-2$^-$). Bacterial AI-2 was from CFS of *V. alginolyticus* ZJO strain while host AI-2 mimic produced by co-culture of *V. alginolyticus* Δ*luxS* with FHM cells. The binding affinity was evaluated using MST analysis. Data are pooled from $n = 3$ independent experiments. The K_d values: Bacterial AI-2, 160 ± 29 nM; Host AI-2 mimic, 171 ± 21 nM

phosphorylation with mono-culture CFS from host cells or the Δ*luxS* strain alone, but ArcB phosphorylation was evident for the co-cultured CFS (Fig. 5D). These data demonstrated that a functional analogue of AI-2 is produced by host cells to stimulate ArcB phosphorylation and its production requires the co-culture of host cells with *V. alginolyticus*. To determine if this host-derived AI-2 signaling phenotype is more generally applicable to *Vibrio* bacteria and other hosts, we co-cultured HeLa cells with *V. parahaemolyticus* (Fig. S4B and C). Findings from this experiment are consistent with the presence of a presumptive host-derived AI-2 functional analogue that contributes to LuxQ-regulated T3SS1 cytotoxicity (Fig. S4B and C).

To determine whether host cells require direct contact with bacteria to produce AI-2 functional analogue, a transwell apparatus was used for indirect contact co-culture, in which the Δ*luxS* strain was cultured in the upper chamber of the transwell above the host cells. After incubation, the CFSs were collected to evaluate bioluminescence. The results showed that AI-2 activity was the same regardless of direct or indirect bacterial contact (Fig. S4D), indicating that host cells do not need physical interaction with bacteria to produce the AI-2 functional analogue. In contrast, T3SS1-induced cytotoxicity required cell contact (Fig. S4E), suggesting that the trigger for AI-2 analogue production is unrelated to *Vibrio* cytotoxicity. We further examined the AI-2 activity in host cells infected with ZJO Δ*luxS*, the non-cytotoxic strain ZJO Δ*luxS*Δ*vscC*, and *E. coli* DE3 Δ*luxS*. All strains induced host production of the AI-2 functional analogue

(Fig. S4F), confirming that T3SS-mediated cytotoxicity is not the trigger. Instead, this response appears to be a general host reaction to bacterial infection.

To verify that ArcB interacts with host-derived AI-2 functional analogue in vitro, purified exArcB without bacterial AI-2 binding was incubated with the CFS from the co-culture of Δ*luxS* and host cells, and then re-purified again. The re-purified exArcB was denatured by heating to release the bound molecules in the supernatant. The bioluminescence assay showed that the above supernatant could induce luminescence in *V. harveyi* reporter strain, consistent with ArcB binding host-derived AI-2 functional analogue (Fig. 5E). As a negative control, LuxO was substituted for the same procedures, showing no AI-2 binding activity. To further clarify the similarity between the AI-2 and functional analogue, HPLC analysis was performed for the DPD/AI-2 standard and the bound molecules released from re-purified exArcB. Both samples displayed a peak at the same retention time. The peak appears at 4.1 min with absorption at 280 nm. Therefore, the AI-2 functional analogue has a similar structure to AI-2, consistent with an AI-2 mimic (Fig. 5F). The direct binding of ArcB with bacterial AI-2 or host AI-2 mimic was further demonstrated using a microscale thermophoresis (MST) assay. The binding analysis revealed that exArcB binds to bacterial AI-2 or host AI-2 mimic with dissociation constants (K_d) of 160 ± 29 nM and 171 ± 21nM, respectively (Fig. 5G), confirming that bacterial AI-2 and host AI-2 mimic are high-affinity ligands for ArcB. Based the above results, we concluded that ArcB senses not only bacterial AI-2, but also host-derived AI-2 mimic, which subsequently trigger phosphotransfer cascade in the ArcB-LuxU-LuxO pathway to regulate *V. alginolyticus* T3SS.

ArcB-LuxU-mediated cytotoxicity is specific to the *V. alginolyticus* strain

A recent study reported that ArcB regulates T3SS1 cytotoxicity in *V. parahaemolyticus* type strain RIMD2210633, but in this case ArcB orchestrates the QS SK LuxQ and RR LuxO by functioning as the Hpt protein [14]. This mechanism is completely different from that we observed in *V. alginolyticus*, where ArcB acts as an SK with the QS Hpt protein LuxU and RR LuxO to regulate T3SS. To explore these differences further, we cross-complemented the *V. alginolyticus* ZJO Δ*arcB* mutant with the *arcB* from *V. parahaemolyticus* RIMD. The cytotoxicity assay found that the *V.p* RIMD *arcB* orthologue could restore cytotoxicity of the *V.a* ZJO Δ*arcB* mutant (Fig. 6A). Interestingly, further investigation revealed that only the N-terminus of the *V.p* RIMD *arcB* ($arcB^{\Delta Hpt}$) was necessary to restore cytotoxicity (Fig. 6B). Complementing *V.p* RIMD Δ*arcB* with *V.a* ZJO *arcB* restored cytotoxicity (Fig. 6C), but only the Hpt domain of *V.a* ZJO *arcB* ($arcB^{Hpt}$) was required for complementation (Fig. 6D). These data suggest that the complemented ArcB orthologues retain their original functional roles in the phosphate cascade by acting as Hpt proteins in *V. parahaemolyticus* and as kinases in *V. alginolyticus*. In contrast, complementing *V.a* ZJO Δ*luxU* with *V.p* RIMD *luxU* failed to restore cytotoxicity (Fig. 6E).

Given that ArcB-LuxU-mediated cytotoxicity in *V. alginolyticus* is dependent on phosphotransfer cascade, we next examined the effects on phosphorylation when cross-complementing ArcB or LuxU from the two *Vibrio* species. In *V.a* ZJO, phosphorylation of the *V.p* RIMD *arcB* occurred when complemented in Δ*arcB* (Fig. 6F), whereas *V.p* RIMD *luxU* complemented in Δ*luxU* was not phosphorylated (Fig. 6G). In *V.p* RIMD, *V.a* ZJO *arcB* complemented in Δ*arcB* was phosphorylated, and this phosphorylation required the presence of LuxQ (Fig. 6H), consistent with the phosphorylation mechanism of the native ArcB. However, *V.a* ZJO *luxU* could not be phosphorylated in *V.p* RIMD Δ*luxU* (Fig. 6I). These results suggest that while the ArcB orthologues in *Vibrio* spp. may be structurally similar, their functional specificity depends on the species-specific cellular context. Therefore, ArcB-LuxU-mediated cytotoxicity is specific to *V. alginolyticus*.

Discussion

Quorum sensing (QS) is a cell density-dependent signaling mechanism that allows bacteria to synchronize gene expression in response to population density by detecting extracellular signaling molecules called autoinducers (AIs) [28]. These AIs are recognized by specific receptors, some of which are integral components of two-component systems (TCSs). TCSs consist of a sensor kinase (SK) and a cognate response regulator (RR) and serve as the primary mechanism for bacterial responses to environmental stimuli, being ubiquitous across the bacterial kingdom [10]. Furthermore, SKs can function with multiple RRs, in essence leading to mixed pathways, or "cross-talk" that has been detected widely in bacteria [38, 39].

The regulatory connection between ArcB, the HK of the anoxic redox control TCS ArcAB, and QS under aerobic conditions has been described previously for *V. parahaemolyticus* [14]. The *V. parahaemolyticus* QS signaling system is composed of membrane sensor receptors LuxN, LuxQ, and CqsS that detect their cognate AIs, and then phosphorylate downstream LuxU and LuxO through a phosphorelay cascade leading to synthesis of the master QS regulators AphA and OpaR to regulate T3SS1 gene expression [12]. In the presence of host cells, however, there is cross-talk whereby ArcB replaces LuxU to connect LuxQ and LuxO thereby triggering changes in T3SS activity. *V. alginolyticus* has a QS signaling system similar to *V. parahaemolyticus* whereby ArcB regulates the T3SS through crosstalk with QS under aerobic conditions. Importantly, however, in this context the *V. alginolyticus* ArcB acts as an SK, forming a regulatory cascade with LuxU and LuxO.

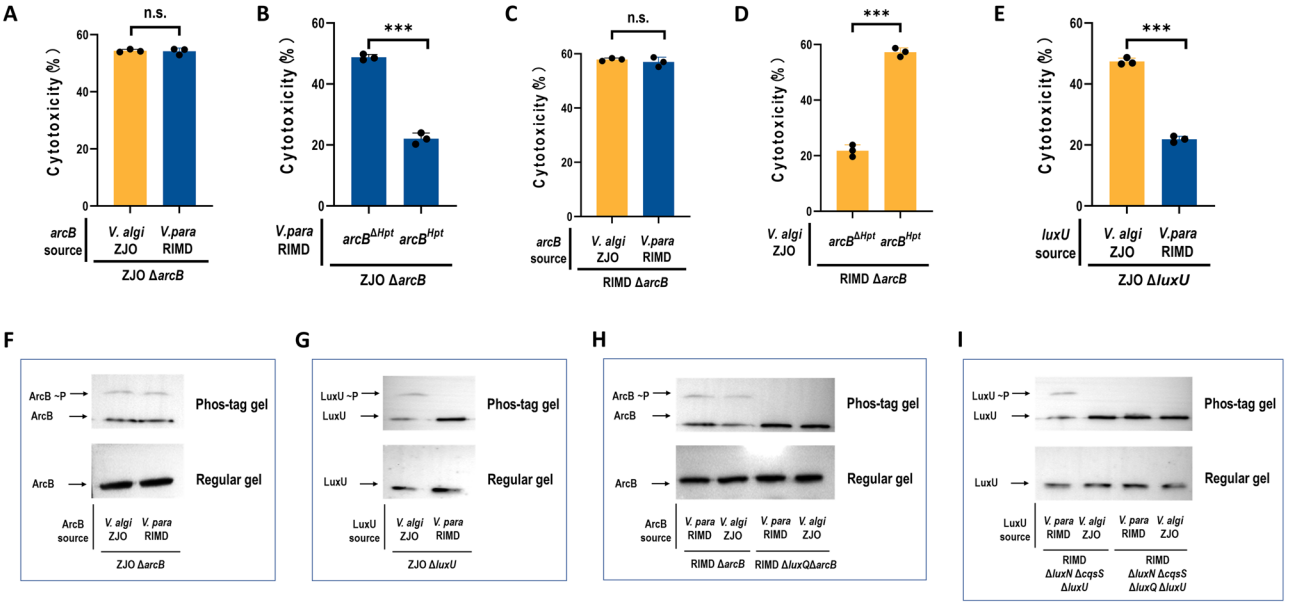

Fig. 6 ArcB-LuxU-mediated cytotoxicity is specific to the *V. alginolyticus* strain. LDH release assays (% cytotoxicity) of FHM cells infected with: **(A)** ZJO Δ*arcB* expressing the *arcB* from indicated sources; **(B)** ZJO Δ*arcB* expressing the N-terminal large region (without Hpt domain) and C-terminal Hpt domain RIMD *arcB*; **(C)** RIMD Δ*arcB* expressing the *arcB* from indicated sources; **(D)** RIMD Δ*arcB* expressing the N-terminal large region (without Hpt domain) and C-terminal Hpt domain of ZJO *arcB*; **(E)** ZJO Δ*luxU* expressing the *luxU* from indicated sources. Yellow: genes derived from *V. alginolyticus* ZJO strain; Blue: genes derived from *V. parahaemolyticus* RIMD strain. Data are presented as means ± SD from three independent experiments. Statistical significance was determined using unpaired two-tailed *t*-test. ***$P < 0.0005$; n.s. not significant. **(F)** In vivo phosphorylation detection of RIMD ArcB in ZJO Δ*arcB* strain. ZJO ArcB was included as positive control. **(G)** In vivo phosphorylation detection of RIMD LuxU in ZJO Δ*luxU* strain. ZJO LuxU was included as positive control. **(H)** In vivo phosphorylation detection of ZJO ArcB in RIMD Δ*arcB* or Δ*luxQ*Δ*arcB* strain. RIMD ArcB was included as positive control. **(I)** In vivo phosphorylation a detection of ZJO LuxU in RIMD Δ*luxN*Δ*cqsS*Δ*luxU* or Δ*luxN*Δ*cqsS*Δ*luxQ*Δ*luxU* strain. RIMD LuxU was included as positive control. The pMMB207 plasmid was used to express those proteins as described above in **F-I**, and each protein was added a Flag tag to the C-terminus. Phosphorylation band was detected by western blot analysis after separation of phos-tag SDS-PAGE (left panel), and conventional 8% SDS-PAGE was run as a control (right panel). Data shown are representative of three independent experiments with similar results

We sought to understand how crosstalk of ArcB has changed from what was likely a common ancestral state to what is now observed in *V. alginolyticus* and *V. parahaemolyticus*. Through heterologous expression, we found that ArcB in the two *Vibrio* species appears to be functionally identical. In contrast, the heterologous expression of *luxU* did not restore activity. Therefore, LuxU has diverged between the two species, whereas ArcB retains its conserved function. The difference in LuxU between the two species may be due to mutations, including potential gene duplication and mutational divergence, that could explain different crosstalk patterns.

Crosstalk between TCSs might be disadvantageous because messages and responses can become confused, leading to inappropriate cellular responses [40], or it could be adaptive [41, 42]. The conditions needed for successful crosstalk may be complex and dependent on environmental signals and context. For instance, in *Bacillus subtilis*, SK PhoR can activate non-cognate YycF during a phosphate limitation-induced stationary phase [43]. The crosstalk of ArcB with QS in *Vibrio* also occurs under specific physiological conditions (T3SS-inducing conditions), while under anaerobic conditions, ArcB autophosphorylates and phosphorylates its cognate response regulator ArcA, which is not required for cytotoxicity neither for the expression of T3SS. Crosstalk between TCS and QS pathways reveals a new layer of complexity in the mechanisms controlling expression of virulence genes in bacteria. It would be interesting to further explore the factors contributing to crosstalk conditions, including the expression levels of the involved proteins, their activation status, and different growth conditions faced by the bacteria. This knowledge will enrich our understanding of bacterial evolution, adaptation, and pathogenic mechanisms.

The ArcAB is a complex two-component system that mediates regulation of operons implicated in respiratory metabolism. Under anoxic conditions, the SK ArcB autophosphorylates and then phosphorylates cognate RR ArcA that represses many operons involved in aerobic respiration [44]. In this study, we found that the ArcB is still able to autophosphorylate under aerobic conditions and is density-dependent. Further, we confirmed that ArcB can independently recognize the QS molecule AI-2 and activate phosphotransfer. Many bacterial species lack AI-2 receptors LsrB or LuxP, but these bacteria can use AI-2 to regulate physiological functions. It is likely that there are unrecognized AI-2 receptors with low sequence

identity to known receptors [15]. Recently, two receptor families have been identified for proteins that recognize AI-2 [19, 20]. Herein, our characterization of ArcB expands the diversity of recognized AI-2 receptors.

QS molecules not only mediate communication between microorganisms, but also allow communication between bacteria and hosts [45]. AI-2 can activate the NF-$_k$B-mediated inflammatory signaling and alpha-induced protein 9 (TNFSF9) signaling [46, 47]. Conversely, certain host signaling molecules can specifically modulate bacterial QS. For example, several virulence factors in *E. coli* are regulated by QS in response to AI-3, but mammalian catecholamines can substitute for AI-3 and directly influence *E. coli* QS by binding to the QS receptor QseC [48]. Host epithelia can produce QS-like molecules, including an AI-2 mimic, enabling interference with bacterial QS circuits [21]. A subsequent study has shown that AI-2 mimic molecules are not exclusive to mammalian epithelial cells. Indeed, under stress conditions, *Saccharomyces cerevisiae* produces an AI-2 mimic called MHF [22]. Herein, we found that host cells release an unidentified signaling molecule during co-culture with bacteria. This novel signaling molecule functions like an AI-2 mimic whereby it is recognized by ArcB to initiate upregulation of T3SS activity. This may be the reason why co-culture, but not physical contact, is sufficient to upregulate the transcription of *V. alginolyticus exsA*.

Conclusions

We found that ArcB functions as a sensor kinase in *V. alginolyticus*, recognizing bacterial AI-2 and an uncharacterized host AI-2 mimic (Fig. 7). At low cell densities,

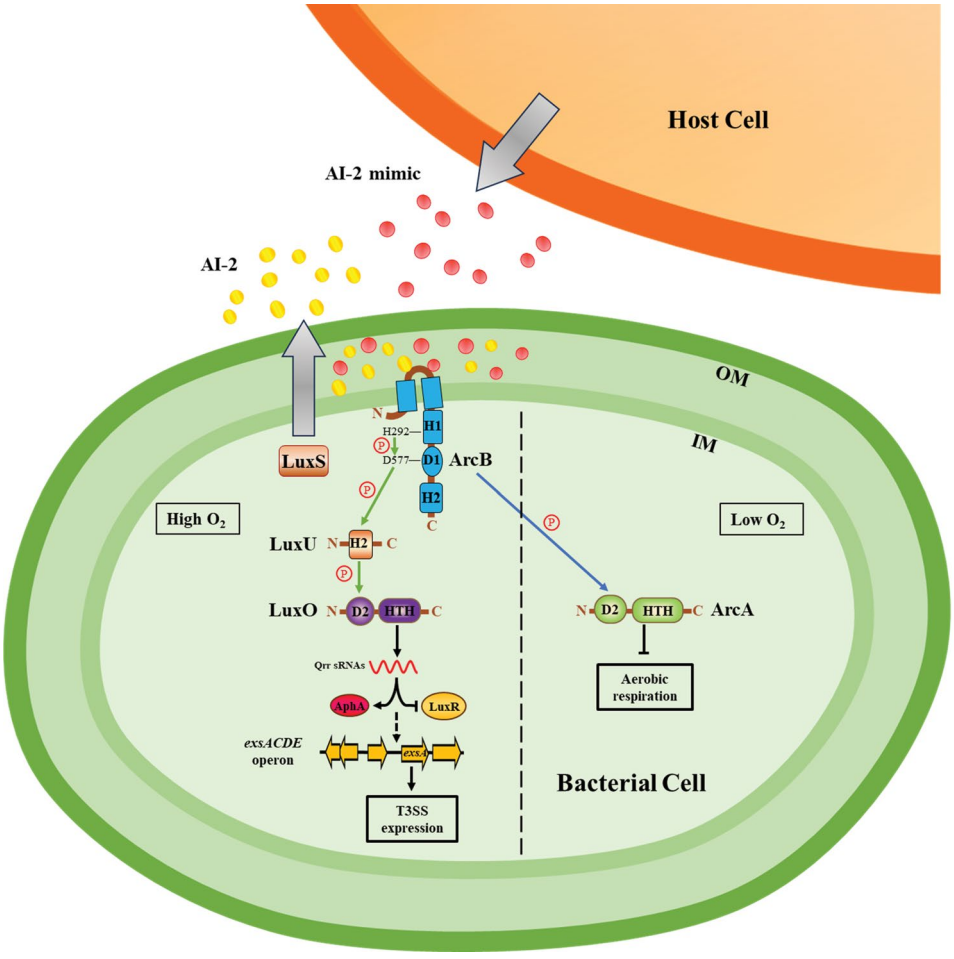

Fig. 7 Models of how the novel ArcB-LuxU-LuxO pathway regulates T3SS in *V. alginolyticus* through sensing bacterial QS AI-2 and host AI-2 mimic. Under high oxygen conditions (left side), the ArcB, a hybrid sensor kinase harboring a HisKA domain (H1), an REC domain(D1), a C-terminal Hpt domain(H2) and two transmembrane domains in *V. alginolyticus*, recognizes the bacterial QS signal AI-2 and host-derived AI-2 mimic, and then initiates autophosphorylation at H292 within the HisKA domain. Subsequently, phosphoryl group transfer occurs orderly at D577 within the REC domain of ArcB, H of LuxU, D of LuxO, eventually causing the phosphorylation of LuxO, then phosphorylated LuxO exerts regulation of T3SS expression by controlling the *exs*ACDE operon. Under low oxygen conditions (right side), the ArcB functions the canonical role that regulates the anaerobic respiration. Green arrows indicate phosphoryl group transfer under high oxygen conditions, while the blue arrow indicates the transfer of phosphate groups under low oxygen conditions. Abbreviations: H, histidine; D, aspartate; HTH, helix-turn-helix; OM, outer membrane; IM, inner membrane

ArcB autophosphorylates the conserved histidine residue within its sensor kinase domain. The phosphoryl group is then guided to the conserved aspartate residue in the attached REC domain, followed by relay to a conserved histidine residue in the Hpt protein LuxU. In the final step of the phosphorylation cascade, the phosphoryl group is transferred from LuxU to a conserved aspartate residue in RR LuxO, triggering the activation of genes encoding Qrr sRNAs [12]. The Qrr sRNAs, in turn, post-transcriptionally activate production of AphA, and AphA ultimately initiates T3SS by activating *exsA*. Elucidation of the ArcB-LuxU-LuxO signaling cascade and its downstream regulatory network has deepened our understanding of how *V. alginolyticus* orchestrates virulence gene expression. The discovery of host-derived AI-2 mimic underscores the intricate dynamics of host-pathogen interactions, revealing that a unique strategy whereby bacteria exploit host signals to modulate infectivity. These findings provide new insights into host-derived molecules that influence bacterial behavior and provide a foundation for exploring bacterial signaling pathways as novel targets for antimicrobial therapies.

Abbreviations

AB	Autoinducer bioassay
AIs	Autoinducers
CFS	Cell-free supernatants
DMEM	Dulbecco's modified Eagle's medium
FBS	Fetal bovine serum
FHM	Fathead minnow
HI	Heart infusion
HisKA	Histidine kinase A
HPLC	High-performance liquid chromatography
Hpt	Histidine phosphotransfer
IPTG	Isopropyl-β-D-thiogalactoside
LB	Luria-Bertani
LDH	Lactate dehydrogenase
MOI	Multiplicity of infection
MST	Microscale thermophoresis
ONPG	O-nitrophenyl-β-D-galactoside
ORF	Open reading frame
PBS	Phosphate-buffered saline
QS	Quorum sensing
REC	Receiver
RR	Response regulator
SK	Sensor kinase
SOE	Splice-overlap-extension
T3SS	Type III secretion system
TCBS	Thiosulfate citrate bile salts
TCS	Two-component system
TSB	Trypticase soy broth

Supplementary Information

The online version contains supplementary material available at https://doi.org/10.1186/s12964-025-02258-0.

Supplementary Material 1: Supplementary figure 1 (Figure S1). (A) Schematic diagram of sensor kinase in ***V. alginolyticus***. A total of 41 new sensor kinases were identified in ***V. alginolyticus***. (B) LDH release assays (% cytotoxicity) of FHM cells infected with sensor kinases mutant strains for 2 h. Data are presented as means ± SD from three independent experiments. Statistical significance was determined using one-way ANOVA. ***P < 0.005. Supplementary figure 2 (Figure S2). (A) Schematic diagram of ***V. alginolyticus*** ArcB, LuxU and LuxO. (B) Measurement of caspase-3 activity. FHM cells were infected with different strains and then collected to measure levels of cleaved caspase substrates. Data are expressed as fold-increase compared to caspase activity in uninfected cells. Data are presented as means ± SD from three independent experiments. Statistical significance was determined using unpaired two-tailed ***t***-test. ***P < 0.0005. Supplementary figure 3 (Figure S3). Expression levels (qRT-PCR) for T3SS genes ***vseE***, ***1686***, ***1687***, ***vopB***, ***vopD*** and ***exsD*** in the indicated strains. Data were normalized to ***rpoA*** expression. The pBBR1MCS-1 plasmid was used for all the complemented strains. Data are presented as means ± SD from three independent experiments. Statistical significance was determined using one-way ANOVA. *P < 0.05; **P < 0.005; ***P < 0.0005; n.s. not significant. Supplementary figure 4 (Figure S4). (A) WT (circle), Δ***luxS*** (triangle), and Δ***arcB***Δ***luxS*** (square) were grown in TSB at 30 °C; growth curves of indicated strains were plotted. All assays were performed in triplicates at least three times. Error bars represent means ± SD. (B) AI-2 activity assays for CFSs from co-cultures of HeLa cells with ***V. parahaemolyticus*** RIMD WT and Δ***luxS*** strains using the AI-2 reporter ***V. harveyi*** strain BB180. As control, ***V. parahaemolyticus*** WT and Δ***luxS*** strains were also cultured in DMEM medium and their CFSs were included. A 5 μM DPD/AI-2 solution served as a positive control. Data are presented as means ± SD from three independent experiments. Statistical significance was determined using one-way ANOVA. ***P < 0.0005. (C) LDH release assays (% cytotoxicity) of HeLa cells infected with the indicated strains under different conditioned culture media for 2 h. Upon infection, the cell culture media were immediately replaced by the CFS from ***V. parahaemolyticus*** Δ***luxS*** mono-culture (blue bars), HeLa mono-culture (pink bars) or co-culture (purple bars). Replace the normal medium (yellow bars) as the control. Data are presented as means ± SD from three independent experiments. Statistical significance was determined using two-tailed multiple ***t***-test. ***P < 0.0005; n.s. not significant (D) Physical contact of ***V. alginolyticus*** with host cells is not necessary for producing the host AI-2 functional analogue. The ***V. alginolyticus*** Δ***luxS*** strain was directly or indirectly (transwell) co-cultured with FHM cells, and their CFSs were collected for measuring bioluminescence production using the reporter strain BB180. A 5 μM DPD/AI-2 solution was included as a positive control. Data are presented as means ± SD from three independent experiments. Statistical significance was determined using one-way ANOVA. ***P < 0.0005. (E) LDH release assays (% cytotoxicity) of ***V. alginolyticus*** WT and Δ***luxS*** strains directly (yellow bars) or indirectly (blue bars) co-cultured with FHM cells. Data are presented as means ± SD from three independent experiments. Statistical significance was determined using one-way ANOVA. ***P < 0.0005. (F) AI-2 activity assays for CFSs from co-cultures of FHM cells with ***V. alginolyticus*** Δ***luxS***, Δ***vscC***Δ***luxS*** and ***E. coli*** BL21Δ***luxS*** strains using the AI-2 reporter ***V. harveyi*** strain BB180. Uninfected cells were used as controls. Data are presented as means ± SD from three independent experiments. Statistical significance was determined using one-way ANOVA. ***P < 0.0005

Supplementary Material 2

Supplementary Material 3

Acknowledgements

We gratefully acknowledge Prof. Jinxin Liu and his research team from Nanjing Agricultural University for their invaluable assistance with microscale thermophoresis measurements.

Author contributions

Z.Z. and C.Z. conceived and designed the research; C.Z., X.J. and Y.W. performed experiments; Y.S. and F.Y. analyzed the data; C.Z. and Z.Z. wrote the paper with input from all authors; D.R.C. advised on the project and provided comments on the manuscript.

Funding

This work was partially supported by the National Natural Science Foundation of China (31872597), Jiangsu Agricultural Science and Technology Independent Innovation Fund (CX [23]1007), Fundamental Research Funds for the Central Universities (B240205011).

Data availability

The authors confirm that the data supporting the findings of this study are available in figshare at https://doi.org/10.6084/m9.figshare.28491221.

Declarations

Competing interests
The authors declare no competing interests.

Received: 22 March 2025 / Accepted: 20 May 2025
Published online: 28 May 2025

References

1. Galán JE, Lara-Tejero M, Marlovits TC, Wagner S. Bacterial type III secretion systems: specialized nanomachines for protein delivery into target cells. Annu Rev Microbiol. 2014;68:415–38.
2. Puhar A, Sansonetti PJ. Type III secretion system. Curr Biol. 2014;24(17):R784–91.
3. Burdette DL, Yarbrough ML, Orvedahl A, Gilpin CJ, Orth K. *Vibrio parahaemolyticus* orchestrates a multifaceted host cell infection by induction of autophagy, cell rounding, and then cell Lysis. Proc Natl Acad Sci U S A. 2008;105(34):12497–502.
4. Hiyoshi H, Kodama T, Iida T, Honda T. Contribution of *Vibrio parahaemolyticus* virulence factors to cytotoxicity, enterotoxicity, and lethality in mice. Infect Immun. 2010;78(4):1772–80.
5. Piñeyro P, Zhou X, Orfe LH, Friel PJ, Lahmers K, Call DR. Development of two animal models to study the function of *Vibrio parahaemolyticus* type III secretion systems. Infect Immun. 2010;78(11):4551–9.
6. Park KS, Ono T, Rokuda M, Jang MH, Okada K, Idia T, et al. Functional characterization of two type III secretion systems of *Vibrio parahaemolyticus*. Infect Immun. 2004;72(11):6659–65.
7. Zhou X, Shah DH, Konkel ME, Call DR. Type III secretion system 1 genes in *Vibrio parahaemolyticus* are positively regulated by ExsA and negatively regulated by ExsD. Mol Microbiol. 2008;69(3):747–64.
8. Gotoh K, Kodama T, Hiyoshi H, Izutsu K, Park KS, Dryselius R, et al. Bile acid-induced virulence gene expression of *Vibrio parahaemolyticus* reveals a novel therapeutic potential for bile acid sequestrants. PLoS ONE. 2010;5(10):e13365.
9. Zhou X, Konkel ME, Call DR. Regulation of type III secretion system 1 gene expression in *Vibrio parahaemolyticus* is dependent on interactions between ExsA, ExsC, and ExsD. Virulence. 2010;1(4):260–72.
10. Capra EJ, Laub MT. Evolution of two-component signal transduction systems. Annu Rev Microbiol. 2012;66:325–47.
11. Gao R, Stock AM. Biological insights from structures of two-component proteins. Annu Rev Microbiol. 2009;63:133–54.
12. Papenfort K, Bassler BL. Quorum sensing signal-response systems in Gram-negative bacteria. Nat Rev Microbiol. 2016;14(9):576–88.
13. Salmon KA, Hung SP, Steffen NR, Krupp R, Baldi P, Hatfield GW, et al. Global gene expression profiling in *Escherichia coli* K12: effects of oxygen availability and ArcA. J Biol Chem. 2005;280(15):15084–96.
14. Zhang C, Liu M, Wu Y, Li X, Zhang C, Call DR, et al. ArcB orchestrates the quorum-sensing system to regulate type III secretion system 1 in *Vibrio parahaemolyticus*. Gut Microbes. 2023;15(2):2281016.
15. Pereira CS, Thompson JA, Xavier KB. AI-2-mediated signalling in bacteria. FEMS Microbiol Rev. 2013;37(2):156–81.
16. Even-Tov E, Bendori SO, Valastyan J, Ke X, Pollak S, Bareia T, et al. Social evolution selects for redundancy in bacterial quorum sensing. PLoS Biol. 2016;14(2):e1002386.
17. Chen X, Schauder S, Potier N, Van Dorsselaer A, Pelczer I, Bassler BL, et al. Structural identification of a bacterial quorum-sensing signal containing Boron. Nature. 2002;415(6871):545–9.
18. Miller ST, Xavier KB, Campagna SR, Taga ME, Semmelhack MF, Bassler BL, et al. Salmonella typhimurium recognizes a chemically distinct form of the bacterial quorum-sensing signal AI-2. Mol Cell. 2004;15(5):677–87.
19. Zhang L, Li S, Liu X, Wang Z, Jiang M, Wang R, et al. Sensing of autoinducer-2 by functionally distinct receptors in prokaryotes. Nat Commun. 2020;11(1):5371.
20. Li S, Sun H, Li J, Zhao Y, Wang R, Xu L, et al. Autoinducer-2 and bile salts induce c-di-GMP synthesis to repress the T3SS via a T3SS chaperone. Nat Commun. 2022;13(1):6684.
21. Ismail AS, Valastyan JS, Bassler BL. A Host-Produced Autoinducer-2 mimic activates bacterial quorum sensing. Cell Host Microbe. 2016;19(4):470–80.
22. Valastyan JS, Kraml CM, Pelczer I, Ferrante T, Bassler BL. *Saccharomyces cerevisiae* requires *CFF1* to produce 4-Hydroxy-5-Methylfuran-3(2H)-One, a mimic of the bacterial Quorum-Sensing autoinducer AI-2. mBio. 2021;12(2).
23. Xie Z, Shaowen K, Chaoqun H, Zhixiong Z, Shifeng W, Yongcan Z. First characterization of bacterial pathogen, *Vibrio alginolyticus*, for Porites andrewsi white syndrome in the South China sea. PLoS ONE. 2013;8(9):e75425.
24. Austin B. Vibrios as causal agents of zoonoses. Vet Microbiol. 2010;140(3–4):310–7.
25. Baker-Austin C, Oliver JD, Alam M, Ali A, Waldor MK, Qadri F, et al. *Vibrio* spp. Infections. Nat Rev Dis Primers. 2018;4(1):8.
26. Zhao Z, Chen C, Hu CQ, Ren CH, Zhao JJ, Zhang LP, et al. The type III secretion system of *Vibrio alginolyticus* induces rapid apoptosis, cell rounding and osmotic Lysis of fish cells. Microbiol (Reading). 2010;156(Pt 9):2864–72.
27. Liu J, Lu SY, Orfe LH, Ren CH, Hu CQ, Call DR, et al. ExsE is a negative regulator for T3SS gene expression in *Vibrio alginolyticus*. Front Cell Infect Microbiol. 2016;6:177.
28. Girard L. Quorum sensing in *Vibrio* spp.: the complexity of multiple signalling molecules in marine and aquatic environments. Crit Rev Microbiol. 2019;45(4):451–71.
29. Henke JM, Bassler BL. Three parallel quorum-sensing systems regulate gene expression in *Vibrio harveyi*. J Bacteriol. 2004;186(20):6902–14.
30. Chen C, Jin X, Chaoqun H. Phenotypic and genetic differences between opaque and translucent colonies of *Vibrio alginolyticus*. Biofouling. 2009;25(6):525–31.
31. Milton DL, O'Toole R, Horstedt P, Wolf-Watz H. Flagellin A is essential for the virulence of *Vibrio anguillarum*. J Bacteriol. 1996;178(5):1310–9.
32. Kinoshita E, Kinoshita-Kikuta E, Shiba A, Edahiro K, Inoue Y, Yamamoto K, et al. Profiling of protein thiophosphorylation by Phos-tag affinity electrophoresis: evaluation of adenosine 5′-*O*-(3-thiotriphosphate) as a phosphoryl donor in protein kinase reactions. Proteomics. 2014;14(6):668–79.
33. Liang X, Moore R, Wilton M, Wong MJ, Lam L, Dong TG. Identification of divergent type VI secretion effectors using a conserved chaperone domain. Proc Natl Acad Sci U S A. 2015;112(29):9106–11.
34. Livak KJ, Schmittgen TD. Analysis of relative gene expression data using Real-Time quantitative PCR and the 2 – ΔΔCT method. Methods. 2001;25(4):402–8.
35. Surette MG, Bassler BL. Quorum sensing in *Escherichia coli* and *Salmonella typhimurium*. Proc Natl Acad Sci U S A. 1998;95(12):7046–50.
36. Vilchez R, Lemme A, Thiel V, Schulz S, Sztajer H, Wagner-Döbler I. Analysing traces of autoinducer-2 requires standardization of the *Vibrio harveyi* bioassay. Anal Bioanal Chem. 2007;387(2):489–96.
37. Freeman JA, Bassler BL. A genetic analysis of the function of LuxO, a two-component response regulator involved in quorum sensing in *Vibrio harveyi*. Mol Microbiol. 1999;31(2):665–77.
38. Yamamoto K, Hirao K, Oshima T, Aiba H, Utsumi R, Ishihama A. Functional characterization in vitro of all two-component signal transduction systems from *Escherichia coli*. J Biol Chem. 2005;280(2):1448–56.
39. Wellington S, Greenberg EP. Quorum sensing signal selectivity and the potential for interspecies cross talk. mBio. 2019;10(2).
40. Rowland MA, Deeds EJ. Crosstalk and the evolution of specificity in two-component signaling. Proc Natl Acad Sci U S A. 2014;111(15):5550–5.
41. Vemparala B, Valiya Parambathu A, Saini DK, Dixit NM. An evolutionary paradigm favoring cross talk between bacterial Two-Component signaling systems. mSystems. 2022;7(6):e0029822.
42. Agrawal R, Pandey A, Rajankar MP, Dixit NM, Saini DK. The two-component signalling networks of *Mycobacterium tuberculosis* display extensive cross-talk *in vitro*. Biochem J. 2015;469(1):121–34.
43. Howell A, Dubrac S, Noone D, Varughese KI, Devine K. Interactions between the YycFG and PhoPR two-component systems in *Bacillus subtilis*: the PhoR kinase phosphorylates the non-cognate YycF response regulator upon phosphate limitation. Mol Microbiol. 2006;59(4):1199–215.
44. Georgellis D, Kwon O, Lin EC. Quinones as the redox signal for the Arc two-component system of bacteria. Science. 2001;292(5525):2314–6.
45. Hughes DT, Sperandio V. Inter-kingdom signalling: communication between bacteria and their hosts. Nat Rev Microbiol. 2008;6(2):111–20.
46. Zargar A, Quan DN, Carter KK, Guo M, Sintim HO, Payne GF, et al. Bacterial secretions of nonpathogenic *Escherichia coli* elicit inflammatory pathways: a closer investigation of interkingdom signaling. mBio. 2015;6(2):e00025.

47. Li Q, Peng W, Wu J, Wang X, Ren Y, Li H, et al. Autoinducer-2 of gut microbiota, a potential novel marker for human colorectal cancer, is associated with the activation of TNFSF9 signaling in macrophages. Oncoimmunology. 2019;8(10):e1626192.
48. Curtis MM, Sperandio V. A complex relationship: the interaction among symbiotic microbes, invading pathogens, and their mammalian host. Mucosal Immunol. 2011;4(2):133–8.

Publisher's note